

**FORWARD OSMOSIS OF WATER ACROSS IONIC MEMBRANES FOR  
DESALINATION**

by

Hao Chen

A thesis submitted to the Faculty of the University of Delaware in partial  
fulfillment of the requirements for the degree of Master of Science in Mechanical  
Engineering

Spring 2020

© 2020 Hao Chen  
All Rights Reserved

**FORWARD OSMOSIS OF WATER ACROSS IONIC MEMBRANES FOR  
DESALINATION**

by

Hao Chen

Approved: \_\_\_\_\_  
Ajay Prasad, Ph.D.  
Professor in charge of thesis on behalf of the Advisory Committee

Approved: \_\_\_\_\_  
Ajay Prasad, Ph.D.  
Chair of the Department of Mechanical Engineering

Approved: \_\_\_\_\_  
Levi T. Thompson, Ph.D.  
Dean of the College of Engineering

Approved: \_\_\_\_\_  
Douglas J. Doren, Ph.D.  
Interim Vice Provost for Graduate and Professional Education and  
Dean of the Graduate College

## **ACKNOWLEDGMENTS**

Firstly, I sincerely appreciate my advisor, Prof. Ajay Prasad for his great patience and support in my master's thesis, he kept guiding me with his wise advice and farsightedness when I lost my direction, without his help, I cannot present this thesis.

Besides my advisor, I would like to thank Xergy Inc. for providing me with all the experimental materials I need, without them, I cannot finish even the simplest experiment. I would also like to thank Prof. Joseph Kuehl and Prof. Bingqing Wei for serving on my thesis committee.

Finally, I would like to thank my friends and colleagues Ashish Chouhan and Tong Wu, they are always willing to help me out when I was stuck in the research.

## TABLE OF CONTENTS

LIST OF TABLES .....	vi
LIST OF FIGURES.....	vii
ABSTRACT.....	x
Chapter	
1 INTRODUCTION TO FORWARD OSMOSIS .....	1
1.1 History of water desalination.....	1
1.2 Goal of the project .....	7
1.3 Organization of the thesis.....	8
2 EXPERIMENT FOR NAFION115 .....	10
2.1 Experiment design for Nafion115.....	10
2.2 List of experiments for Nafion115.....	12
2.3 Data and analysis for Nafion115 .....	13
2.3.1 Data analysis for beaker test .....	14
2.3.2 Data analysis for tank test.....	17
3 FORWARD OSMOSIS EXPERIMENT WITH XERGY MEMBRANES ....	21
3.1 Experimental design.....	21
3.2 Lists of experiments for membrane X.....	21
3.3 Data and analysis for membrane X.....	23
3.3.1 Room temperature test.....	23
3.3.2 Comparison of X-normal with X-special .....	24
3.3.3 Additional tests with X-normal for various PA concentrations..	28
3.3.4 Effect of temperature gradient across the membrane for PA solution .....	32
3.3.5 Effect of temperature gradient across the membrane for ionic liquid (1-Ethyl-3-methylimidazolium acetate, CAS:[143314- 17-4]) .....	35
4 MODELLING OF FORWARD OSMOSIS.....	39
4.1 Basic modelling for experiments in 3.1 .....	39
4.2 Modelling of forward osmosis in a tube flow .....	40
4.3 Effect of parameter variation on simulation results.....	45

5	CONCLUSIONS AND FUTURE WORK .....	48
5.1	Conclusions .....	48
5.2	Future work .....	48
	REFERENCES .....	50
Appendix		
A	MATLAB FUNCTION OF MODELLING USED IN 4.3 .....	52
A.1	Function for varying <b><i>KSW</i></b> and <b><i>KPA</i></b> .....	53
A.2	Function for varying <b><i>Re</i></b> .....	56
B	COPYRIGHT PERMISSION OF FIGURES .....	59

## LIST OF TABLES

Table 2.1 Experiments for Nafion115.....	12
Table 3.1 Preliminary tests for ‘X’ .....	22
Table 3.2 Comparison tests for two kinds of ‘X’ .....	22
Table 3.3 Concentration gradient tests for X-normal.....	22
Table 3.4 Temperature gradient tests for X-normal.....	23
Table 3.5 Repeated tests of temperature gradient for IL.....	23

## LIST OF FIGURES

Figure 1.1 Schematic of MSF <sup>[3]</sup> , A - Steam in; B - Seawater in; C - Potable water out; D - Brine out (waste); E - Condensate out; F - Heat exchange; G - Condensation collection; H - Brine heater .....	2
Figure 1.2 Schematic of multi-effect distillation <sup>[4]</sup> .....	3
Figure 1.3 Single effect vapor compression distillation <sup>[6]</sup> .....	4
Figure 1.4 Working principle of electrodialysis <sup>[8]</sup> .....	5
Figure 1.5 Working principle of reverse osmosis <sup>[9]</sup> .....	6
Figure 1.6 Concept of solar desalination using forward osmosis with vacuum membrane pervaporation. The focus of this thesis is the forward osmosis step (shown by the dashed line box).....	8
Figure 2.1 Experimental setup for Nafion115 on a counter-top at room temperature. ....	10
Figure 2.2 Experimental setup for Nafion115 in an oven at 40°C.....	11
Figure 2.3 Tank test with magnetic stirrer and Nafion115.....	13
Figure 2.4 Mass of liquid inside the jar versus time for the beaker test with Nafion115 for 22 and 40°C, and initial PA concentrations of 25% and 33%. .....	14
Figure 2.5 PA concentration versus time for the beaker test at room temperature with Nafion115. The 25% curve is offset from the 33% curve by 16 hours.....	15
Figure 2.6 PA concentration versus time for the beaker test at 40°C with Nafion115. The 25% curve is offset from the 33% curve by 16 hours... ..	16
Figure 2.7 Flux versus time for the beaker test at room temperature with Nafion115. The 25% curve is offset from the 33% curve by 16 hours... ..	16
Figure 2.8 Flux versus time for the beaker test at 40°C with Nafion115. The 25% curve is offset from the 33% curve by 16 hours.....	17
Figure 2.9 Mass of liquid inside the jar versus time for the tank test with Nafion115 at 22°C for PA concentrations of 25% and 33%. .....	17

Figure 2.10 PA concentration versus time for the tank test at room temperature with Nafion115. The 25% curve is offset from the 33% curve by 22 hours...	18
Figure 2.11 Flux versus time for the tank test at room temperature with Nafion115. The 25% curve is offset from the 33% curve by 22 hours.....	18
Figure 2.12 Comparison of flux versus time curves for the beaker test (BT) and tank test (TT) at room temperature with Nafion115. No time offsets are employed here.....	19
Figure 3.1 Preliminary tests for X-normal at room temperature (22°C).....	24
Figure 3.2 Water transferability for X-normal at 22°C and 50°C.....	25
Figure 3.3 Water transferability for X-special at 22°C and 50°C.....	25
Figure 3.4 Concentration versus time for both X membranes at RT and 50°C; all experiments employed 66.7% PA solution with 3% saltwater.....	27
Figure 3.5 Flux versus time for both X membranes at RT and 50°C; all experiments employed 66.7% PA solution with 3% saltwater.....	27
Figure 3.6 Additional tests with X-normal at 22°C, initial weight of liquid was set to 40g.....	28
Figure 3.7 Additional tests with X-normal at 40°C, initial weight of liquid controlled at 40g.....	29
Figure 3.8 Concentration versus time for X-normal at room temperature group and 40°C.....	30
Figure 3.9 Flux versus time for X-normal at room temperature group and 40°C.....	31
Figure 3.10 Dilution of PA solution versus time for two situations: (1) both saltwater and PA solution heated, and (2) only saltwater heated.....	32
Figure 3.11 Concentration versus time comparing “both SW and PA at 40°C” and “SW at 40°C, PA at RT” cases for X-normal.....	33
Figure 3.12 Flux versus time comparing “both SW and PA at 40°C” and “SW at 40°C, PA at RT” cases for X-normal.....	34
Figure 3.13 Dilution of ionic liquid versus time for four situations: (1) both IL and SW at room temperature; (2) both IL and SW at 40°C; (3) IL at RT, SW at 40°C; and (4) IL at 40°C, SW at 40°C.....	35

Figure 3.14 Flux versus time for four cases with X-normal and ionic liquid.....	36
Figure 4.1 Experimental setup in 3.1 (top); and water flux across the membrane driven by pressure difference (bottom), $\pi_{PA}$ and $\pi_{SW}$ represent the osmotic pressures in PA and SW solutions, respectively.....	39
Figure 4.2 Schematic of tube flow for modeling purposes .....	41
Figure 4.3 Analysis of forward osmosis in a tube flow. $C_{20}$ and $C_{2i}$ represent the bulk and interfacial water concentration on the SW side, respectively. $C_{10}$ and $C_{1i}$ represent the bulk and interfacial water concentration on the PA side. $R$ is the tube radius. $C_n$ and $C_{n+1}$ represent the concentration of PA ( $\text{g}/\text{cm}^3$ ) at the entry and exit of the control volume, respectively. $u_{c,n}$ represents the velocity of water entering the control volume across the tube wall. $u_n$ and $u_{n+1}$ represent the velocity of PA solution flow at the entry and exit of the control volume, respectively. ....	42
Figure 4.4 Profiles of $C_m(x)$ for varying $K_{SW}$ and $K_{PA}$ for $Re = 10$ . ....	46
Figure 4.5 Profiles of $C_m(x)$ for varying $Re$ for $K_{SW} = K_{PA} = 10 - 3 \text{ cm/s}$ ...	47

## ABSTRACT

Although 70% of the earth is covered by water, only 3% is available for consumption in daily human life or for industrial use. With the sharp rise in population over recent decades, the growing demand for fresh water has led to water scarcity and water stress. As a result, a total of 2.7 billion people suffer from water scarcity for at least one month per year<sup>[1]</sup>. The lack of pure water has threatened the development of many countries and motivates us to seek novel approaches to obtain pure water via the desalination of seawater. These can be mainly divided into two categories, one using membranes, and the other using evaporation. Here, we focus on a membrane-based method to purify seawater, i.e. forward osmosis.

The objective of this thesis is to test the effectiveness of an ionic liquid to draw water from a saltwater solution across an ionic membrane by forward osmosis. Due to the high cost of ionic liquid, most of the experiments were conducted with Potassium Acetate solution which is thought to have similar physical properties to ionic liquid. Forward osmosis experiments were conducted using a baseline Nafion115 membrane as well as proprietary membranes supplied by Xergy Inc. Water transport was measured at varying temperatures and concentrations of Potassium Acetate solution. These measurements were then used to create a simple model for the design of a shell-and-tube mass exchange apparatus.

## **Chapter 1**

### **INTRODUCTION TO FORWARD OSMOSIS**

Although 70% of the earth is covered by water, only 3% is available for consumption in daily human life or for industrial use. With the sharp rise in population over recent decades, the growing demand for fresh water has led to water scarcity and water stress. As a result, a total of 2.7 billion people suffer from water scarcity for at least one month per year<sup>[1]</sup>. The lack of pure water has threatened the development of many countries and motivates us to seek novel approaches to obtain pure water via the desalination of seawater. These can be mainly divided into two categories, one using membranes, and the other using evaporation. These techniques are reviewed in the following sections.

#### **1.1 History of water desalination**

Water desalination has been employed to obtain fresh water for many decades. The two most common methods for water desalination are distillation and osmosis. Distillation methods can be classified into three types: multi-stage flash distillation (MSF), low temperature multi-effect distillation (LT-MED), and pressure distillation. The osmosis method which employs membranes can also be classified into three types: electrodialysis, forward osmosis (FO), and reverse osmosis (RO).

### Distillation Methods:

As shown in Figure 1.1, multi-stage flash distillation introduces seawater into a flash chamber after it is heated to a certain temperature<sup>[2]</sup>. The pressure in the chamber is lower than the saturated vapor pressure corresponding to the sea water. Therefore, some of the seawater evaporates rapidly due to the pressure difference and the condensate is collected as pure water. The remaining seawater is then introduced to the next chamber with a lower pressure than the first chamber, and the process of evaporation and condensation is repeated. Several such flash chambers are connected in series, wherein the pressure in the chamber and the seawater temperature decreases step by step, and potable water is continuously produced.

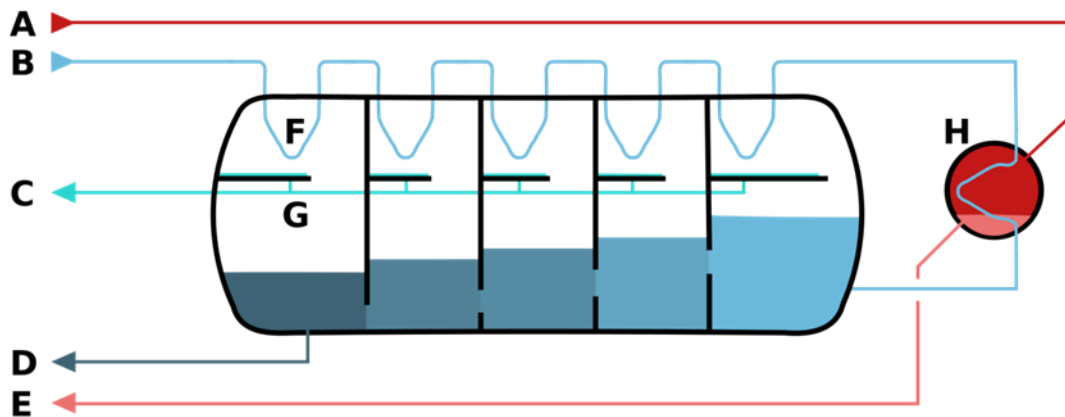


Figure 1.1 Schematic of MSF<sup>[3]</sup>, A - Steam in; B - Seawater in; C - Potable water out; D - Brine out (waste); E - Condensate out; F - Heat exchange; G - Condensation collection; H - Brine heater

As shown in Figure 1.2, in low temperature multi-effect distillation<sup>[4]</sup>, seawater is divided into two streams, one serving as cooling water and discharged to sea, and

the other for feed to the distillation chambers. After adding an anti-sludging agent, the second flow is sprayed into a low-pressure evaporator which is heated by tubes carrying steam. Some of the seawater evaporates and the condensate is collected as pure water. Some of the vapor is sent into the next chamber to provide heat to the seawater and the process of evaporation and condensation is repeated. Multiple such chambers are connected in series such that the temperature and pressure is successively lowered with fresh water being collected in each chamber.

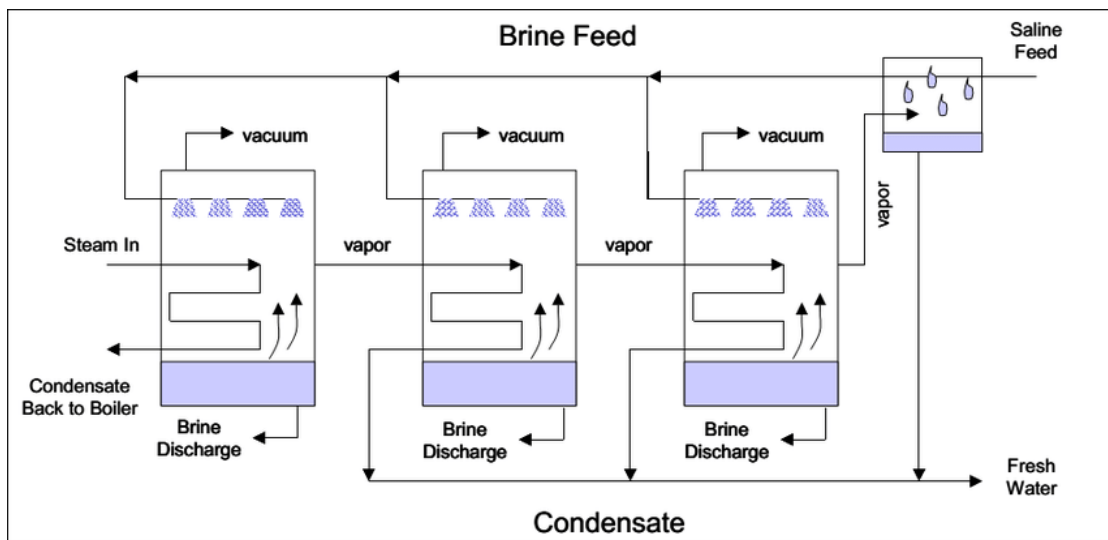


Figure 1.2 Schematic of multi-effect distillation<sup>[4]</sup>.

As shown in Figure 1.3, vapor compression distillation<sup>[5]</sup> is based on the fact that the temperature rises when any gas is compressed. First, seawater is fed to the evaporator to generate water vapor which is then introduced to a compressor resulting in a high temperature steam which serves to heat the seawater. Next, the steam flows into a heat exchanger where it preheats the incoming seawater and condenses to create

potable water.

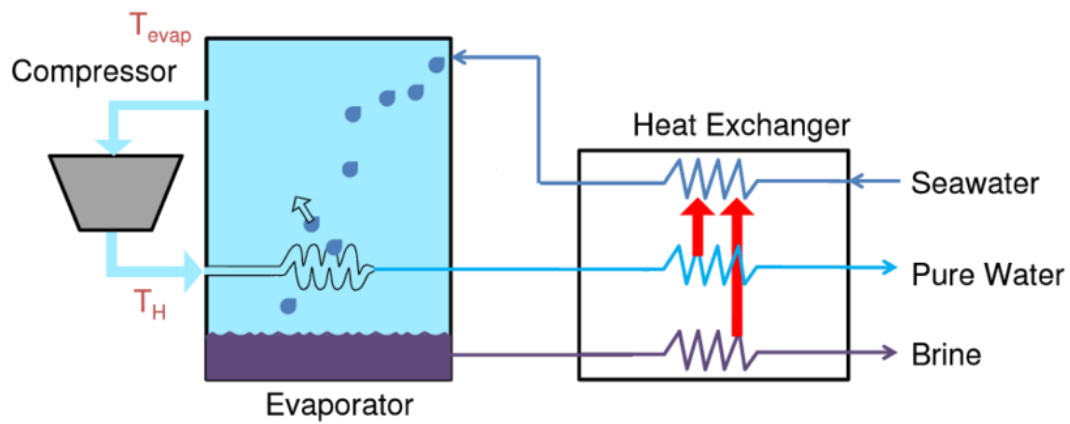


Figure 1.3 Single effect vapor compression distillation<sup>[6]</sup>.

The primary shortcoming of distillation methods is low efficiency and high cost, and there is still no distillation method that can operate continuously for long periods.

#### Membrane-based methods:

The other method which uses membranes can also be classified into three types: electrodialysis, reverse osmosis (RO), and forward osmosis (FO). Membranes represent a newer technology, and after years development this has become the mainstream method instead of evaporation. These methods developed mainly due to the study of membranes such as the ion exchange membrane used in electrodialysis. Due to lower energy cost compared to evaporation, membrane purification has evolved rapidly in recent years.



As shown in Figure 1.5, reverse osmosis (RO)<sup>[9]</sup>, also known as ultrafiltration (UF), uses a semipermeable membrane that allows only solvents to pass through while blocking solutes, thereby separating fresh water from seawater. Normally, osmotic pressure causes freshwater to diffuse through a semipermeable membrane to the seawater side, causing the water level on the seawater side to rise gradually until a certain height before stopping. This process is called infiltration. However, if an external pressure is applied to the seawater side that exceeds the osmotic pressure, then the direction of flow can be reversed such that pure water flows out of the seawater. The biggest advantage of reverse osmosis is that it is energy saving. Its energy consumption is only 1/2 of electrodialysis and 1/40<sup>th</sup> of distillation. Therefore, since 1974, developed countries such as the US and Japan have shifted their focus to reverse osmosis.

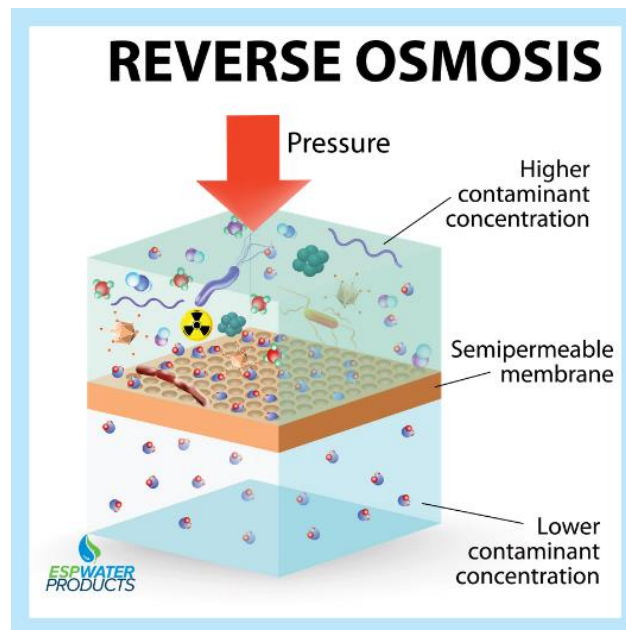


Figure 1.5 Working principle of reverse osmosis<sup>[9]</sup>

Finally, we come to forward osmosis, which represents the main thrust of this thesis. In our application, seawater is separated from an ionic liquid by a semipermeable membrane. Pure water then migrates across the membrane from the seawater side to the ionic liquid. The natural process by which water transfers from a lower concentration solvent to a higher one is called forward osmosis (FO). The role of FO in our proposed desalination method is described next.

## **1.2 Goal of the project**

The overall goal is to employ ionic membranes combined with solar heat to achieve an effective two-step seawater desalination process as shown in Figure 1.6. In the first step, FO is applied to first to draw water from seawater (green loop) through selected membranes into an ionic liquid (EMIMOAc, red loop). In the second step, vacuum pervaporation is used to extract water vapor from the ionic liquid to which is condensed to obtain pure water (blue loop) as shown in Figure 1.6. The focus of this thesis is the Forward Osmosis step. Unlike reverse osmosis, forward osmosis does not consume energy, and is also less susceptible to membrane fouling. Therefore, the feed seawater does not need to be filtered before entering the forward osmosis unit.

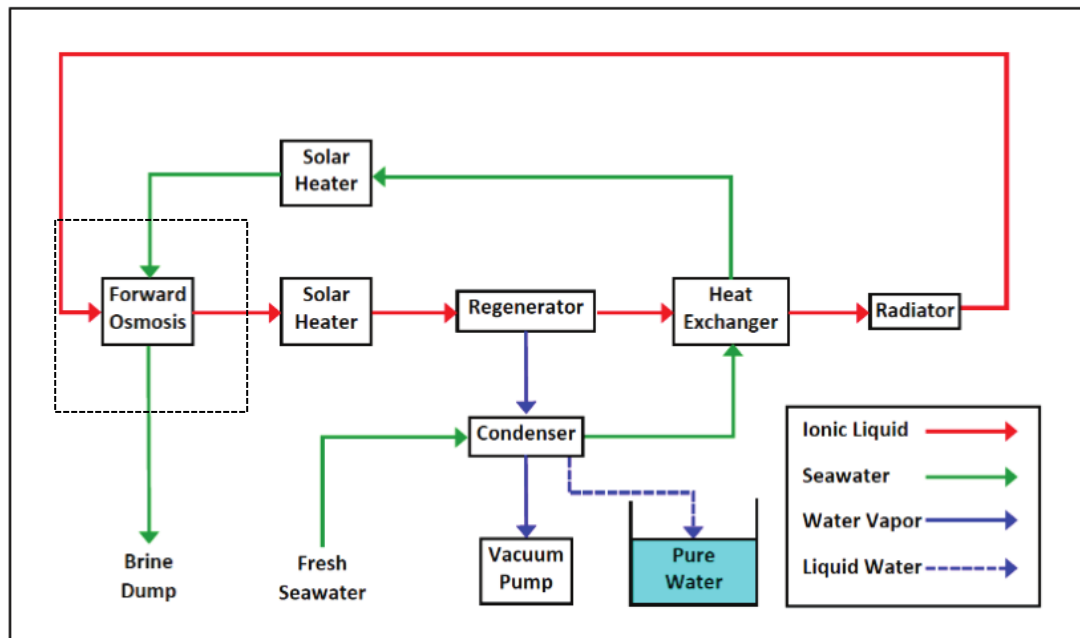


Figure 1.6 Concept of solar desalination using forward osmosis with vacuum membrane pervaporation. The focus of this thesis is the forward osmosis step (shown by the dashed line box).

### 1.3 Organization of the thesis

The key parameter for this thesis is the water transferability of different membranes, which is quantified by the water flux through the membrane between two liquids with different solute concentrations. Two membranes were tested: Nafion115 and a perfluorosulfonic acid membrane (PFSA) from Xergy Inc. Due to the high cost of ionic liquid (\$100 per 100ml), the laboratory standard potassium acetate (\$30 per 500g) solution was used as a surrogate for the ionic liquid and 3% NaCl (common salt) solution was used to represent seawater.

In Chapter 2, we describe baseline experiments with Nafion115 to collect primary data and validate the experimental process before testing with Xergy membranes. Chapter 3 describes experiments with two types of Xergy PFSA

membranes, and results for concentration and flux versus time curves are provided. Chapter 4 presents modelling of forward osmosis for Nafion115 and Xergy membranes based on Fick's law. Chapter 5 summarizes the main conclusions and provides suggestions for future work.

## Chapter 2

### EXPERIMENT FOR NAFION115

#### 2.1 Experiment design for Nafion115

Nafion115 is a mature, commercial membrane widely used in various applications. Forward Osmosis (FO) experiments were first conducted with Nafion115 as a baseline membrane to gather raw data and conduct primary analysis before performing experiments with the Xergy membranes (X).

As shown in Figure 2.1, all the experiments reported here employed 80ml acrylic jars (Beauticom) partially filled with an aqueous solution of potassium acetate (PA). The mouths of the jars were tightly closed by the Nafion115 membrane. A leak tight seal was ensured by using silicone sealant. The jars were then placed in an inverted configuration (membrane facing down) in a 400ml beaker filled with 3% saltwater (by weight) such that the membrane stayed submerged in the beaker. A small hole (1mm diameter) was drilled in the bottom of the jar to balance the pressure inside the jar with the ambient pressure.



Figure 2.1 Experimental setup for Nafion115 on a counter-top at room temperature

Due to the difference in ion concentration on either side of the membrane, water molecules will migrate from the saltwater solution through the membrane into PA by Fickian diffusion. Consequently, the mass of the liquid inside the jar would increase, and the change in mass is equal to the amount of water absorbed. The jar was removed from the beaker every 12 hours, patted dry, and its mass was measured on a scale (U.S. Solid, model #USS-DBS00005).

Primary tests were conducted at room temperature (22°C), and at 40°C in a laboratory oven (see Figure 2.2) to evaluate the effect of temperature on water transport. Some tests were also conducted in a larger tank with a magnetic stirrer to evaluate the effect of convection on the saltwater side. The temperature of 40°C was selected because the eventual goal of the proposed work is to conduct forward osmosis using solar thermal heat (40-60°C).



Figure 2.2 Experimental setup for Nafion115 in an oven at 40°C

## 2.2 List of experiments for Nafion115

Four groups of forward osmosis experiments were conducted by controlling the initial PA concentration and operating temperature:

Table 2.1 Experiments for Nafion115

Temperature (°C)	PA Concentration (%)	Saltwater Concentration (%)
22	25	3
	33	
40	25	
	33	

In the stirred tank test shown in Figure 2.3, the goal was to evaluate the ability of convection to disrupt the concentration boundary layer adjacent to the membrane. A 5L aquarium tank was filled with saltwater, and two experiments with different concentrations (25 and 33%) of PA solution were conducted. A magnetic stirrer (CORNING MODEL PC-420) was employed at a setting of “3” to drive a convective water flow inside the tank.

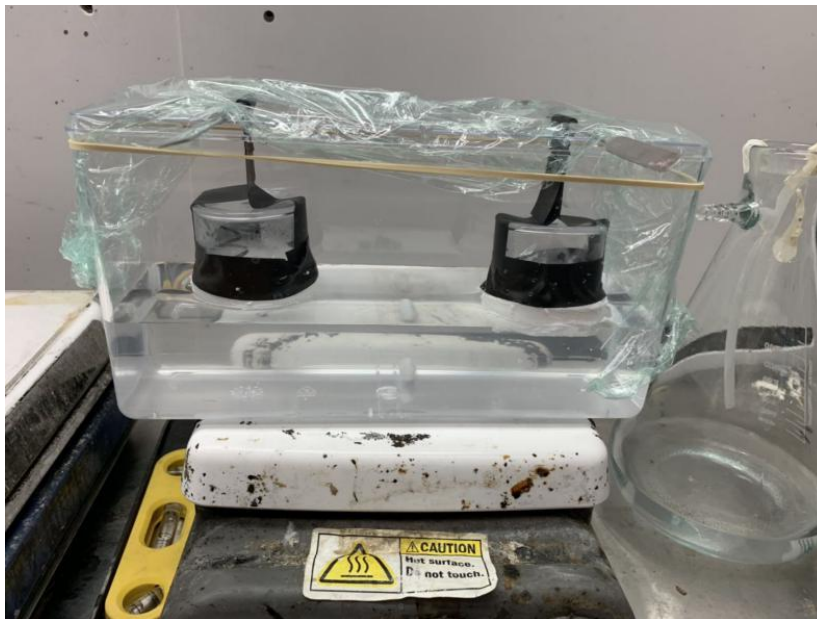


Figure 2.3 Tank test with magnetic stirrer and Nafion115

### 2.3 Data and analysis for Nafion115

For both the beaker and tank tests, the mass of liquid was recorded as a function of time. From this it is possible to calculate the flux of water transferred through Nafion115, and the resulting drop in concentration of the PA solution inside the jar as a function of time.

Due to the thickness of Nafion115 ( $127\mu\text{m}$ ) the rate of water migration across the membrane is small, hence the tests take a long time to complete. Hence, the sampling time was set to 24 hours. The jars were removed from the beaker (or tank) once every day and their weight was measured after patting dry the surface of membrane and the jar. The initial weight of the PA solution in the jar was always set to 15g. The mass of the liquid is plotted as a function of time for the beaker test in Figure 2.4, and for the tank test in Figure 2.5.

### 2.3.1 Data analysis for beaker test

The mass of liquid inside the jar versus time for the beaker test is shown in Figure 2.4. The starting mass of liquid in each test was set at 15 g.

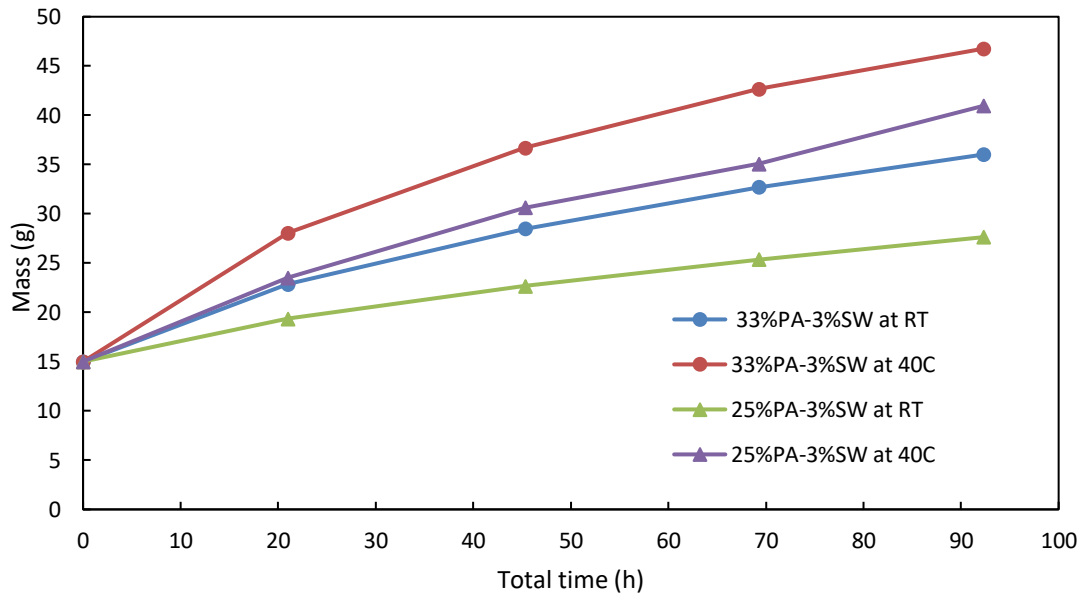


Figure 2.4 Mass of liquid inside the jar versus time for the beaker test with Nafion15 for 22 and 40°C, and initial PA concentrations of 25% and 33%.

Next, we plot both the concentration vs. time and flux vs. time curves. PA concentration is determined as:

$$\text{concentration} = \frac{m_{PA}}{m_L} \quad (1.1)$$

where  $m_{PA}$  is the mass of solute PA in the jar (which remains fixed over time), and  $m_L$  is the total mass of the solution (which increases with time).

The flux of water across the membrane is calculated as:

$$\text{Flux} = \frac{\Delta m}{\Delta t S} \quad (1.2)$$

where  $\Delta m$  is the mass change of liquid inside the jar (= mass of water transferred in g),  $\Delta t$  is the time increment in seconds, and  $S$  is the surface area of the membrane (= 19.625cm<sup>2</sup>).

We plot the PA concentration as a function of time for the beaker tests at 22 and 40°C in Figures 2.5 and 2.6, respectively. The 25% PA concentration curve is offset from the 33% curve by about 16 hours in both Figures 2.5 and 2.6. This offset was obtained by just eye-balling the two curves such that they overlaid each other to the best possible extent. We then plot the water flux vs. time for the beaker test at 22 and 40°C in Figures 2.7 and 2.8, respectively. The same offsets used in the concentration vs. time curves are employed in the flux vs. time curves as well.

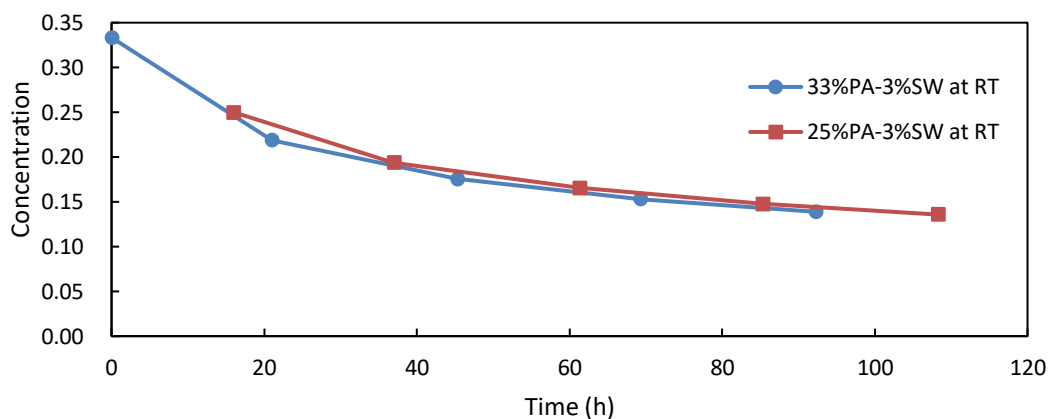


Figure 2.5 PA concentration versus time for the beaker test at room temperature with Nafion115. The 25% curve is offset from the 33% curve by 16 hours.

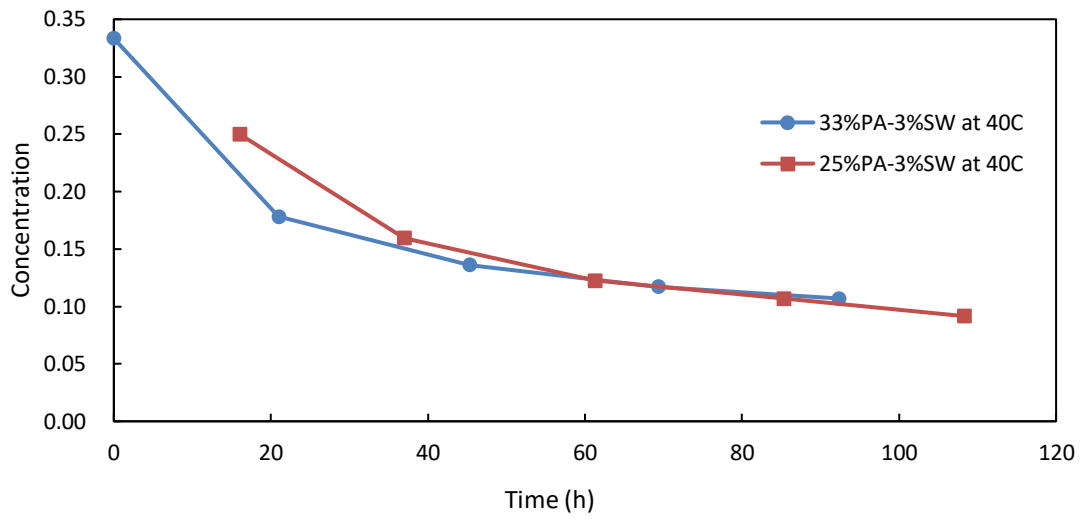


Figure 2.6 PA concentration versus time for the beaker test at 40°C with Nafion115. The 25% curve is offset from the 33% curve by 16 hours.

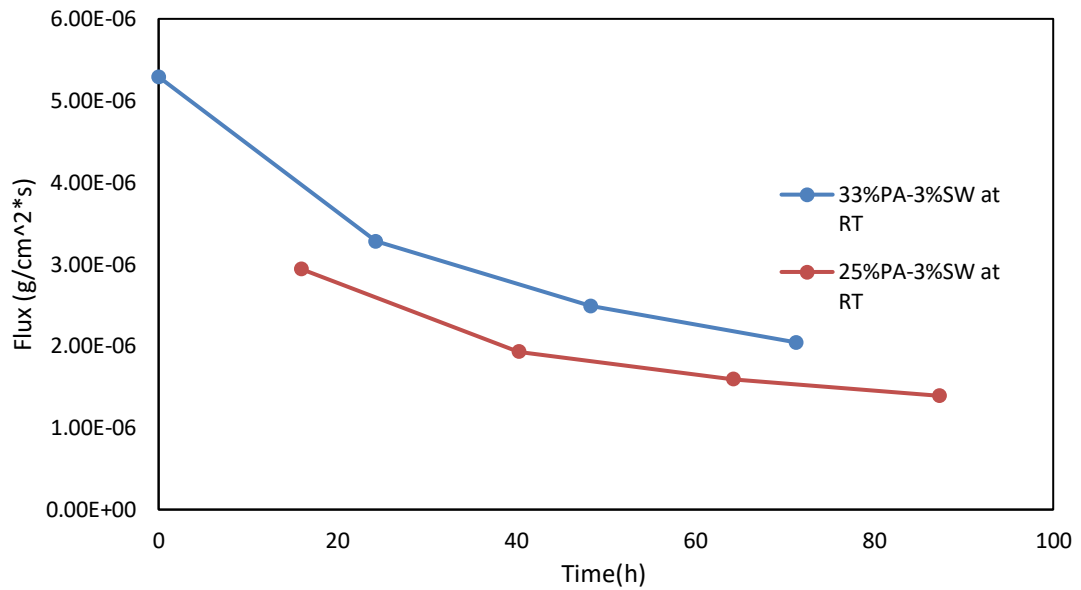


Figure 2.7 Flux versus time for the beaker test at room temperature with Nafion115. The 25% curve is offset from the 33% curve by 16 hours.

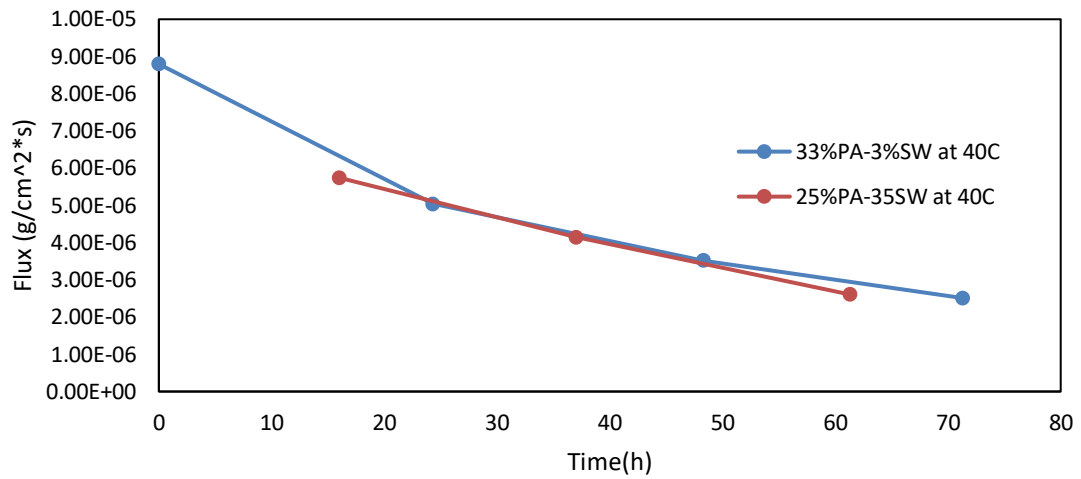


Figure 2.8 Flux versus time for the beaker test at 40°C with Nafion115. The 25% curve is offset from the 33% curve by 16 hours.

### 2.3.2 Data analysis for tank test

We now plot the mass of liquid inside the jar versus time for tank test in Figure 2.9.

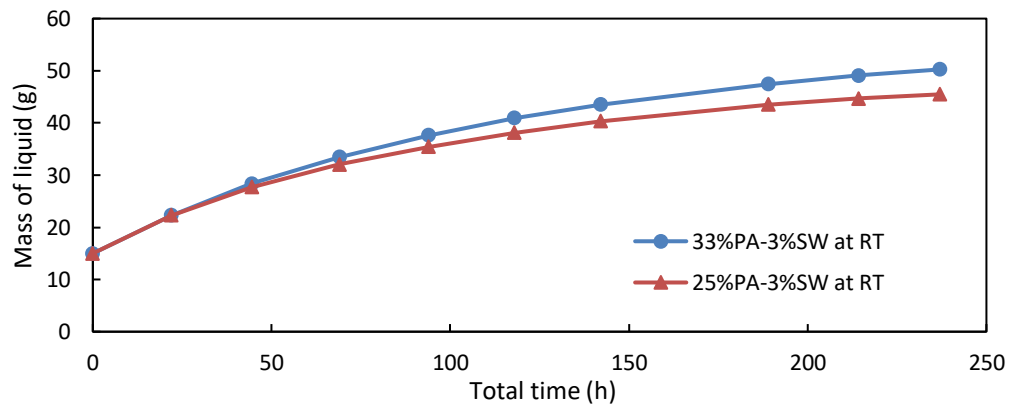


Figure 2.9 Mass of liquid inside the jar versus time for the tank test with Nafion115 at 22°C for PA concentrations of 25% and 33%.

Figures 2.10 and 2.11 show the concentration vs. time and flux vs. time, respectively, for the tank test at room temperature. Here, the 25% PA curve is offset from the 33% curve by about 22 hours.

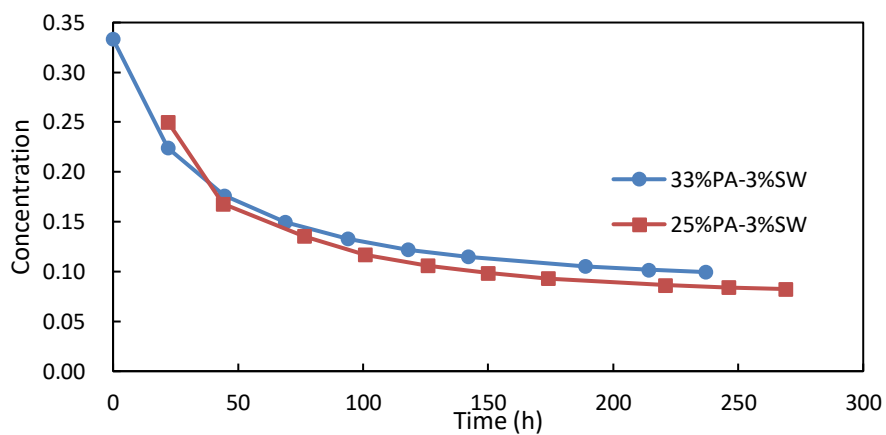


Figure 2.10 PA concentration versus time for the tank test at room temperature with Nafion115. The 25% curve is offset from the 33% curve by 22 hours.

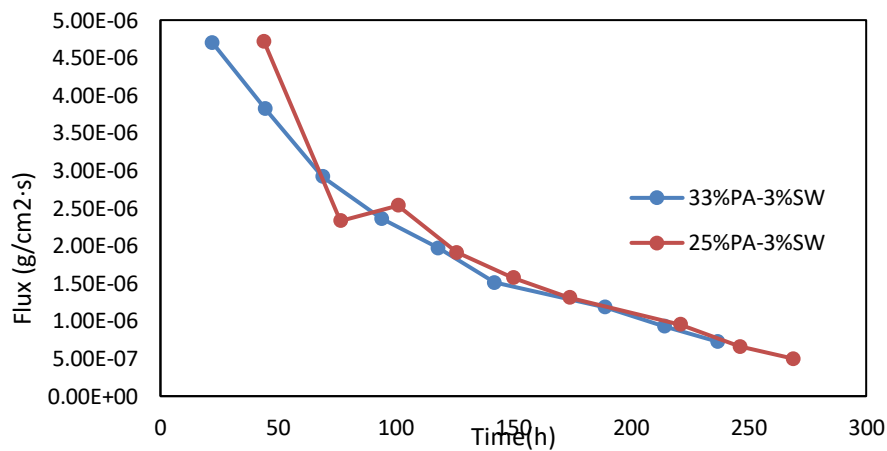


Figure 2.11 Flux versus time for the tank test at room temperature with Nafion115. The 25% curve is offset from the 33% curve by 22 hours

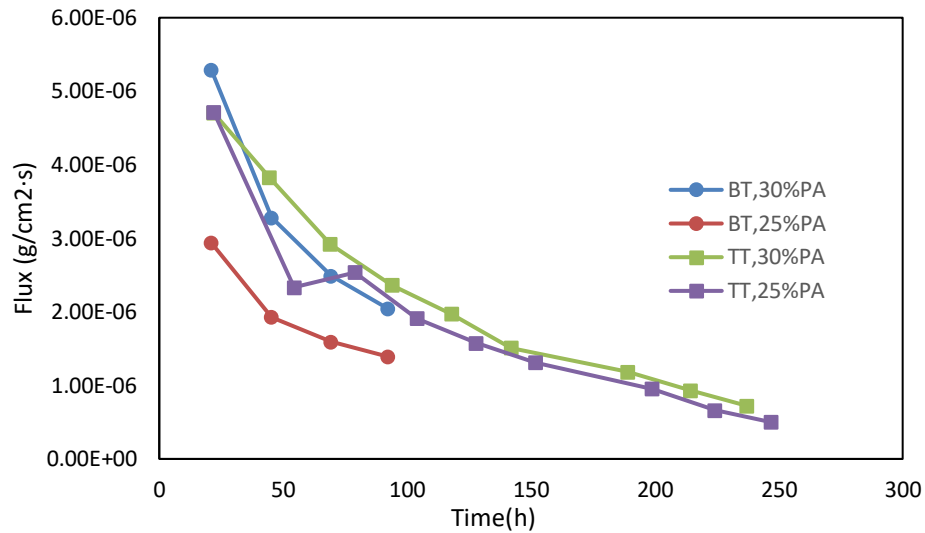


Figure 2.12 Comparison of flux versus time curves for the beaker test (BT) and tank test (TT) at room temperature with Nafion115. No time offsets are employed here.

Now we examine the effect of initial PA concentration, operating temperature, and convection. It is immediately obvious from Figure 2.12 that a higher PA concentration results in a higher water transfer rate. This result is expected. A higher PA concentration implies a lower water concentration and hence a greater water concentration differential that enhances water diffusion across the membrane. It is easily seen in Figure 2.12 that the flux reduces with time, i.e. as the PA solution becomes more dilute. For the effect of temperature, we can compare Figures 2.7 and 2.8 for the beaker test at 22 and 40°C, respectively. The flux is almost twice as high at 40°C. This can be attributed to the higher diffusivity of water in Nafion115 at a higher temperature. Nguyen and White<sup>[10]</sup> provide an expression that relates diffusivity of water in the membrane to the temperature:

$$D = (1.76 \times 10^{-5} + 1.94 \times 10^{-4} \lambda) \exp \left[ \frac{-2436}{T} \right]$$

where  $T$  is the temperature in K, and  $\lambda$  is the number of water molecules per sulfonic acid side chain in the ionomer. For a membrane in contact with liquid water,  $\lambda \approx 22^{[11]}$ .

From Figure 2.12, we can also observe that the flux for the beaker test is slightly smaller than the flux for the tank test. Thus, we may conclude that disrupting the concentration boundary layer on the saltwater side of the membrane has a relatively small beneficial effect on water transport. We can thus infer that the concentration boundary layer comprises only a small portion of the total mass transfer resistance.

## Chapter 3

### FORWARD OSMOSIS EXPERIMENT WITH XERGY MEMBRANES

#### 3.1 Experimental design

Similar to Nafion115, Xergy's perfluorosulfonic acid membrane (PFSA) membrane (hereafter labeled membrane "X") also contains nanometer-sized hydrophilic domains that confer excellent selectivity to water transport while blocking mobile ionic species, such as salts. The main difference between Nafion115 and X is the membrane thickness; Nafion115 has thickness of 127 $\mu\text{m}$ , whereas X has a thickness of only 25 $\mu\text{m}$ . Hence, everything else being equal, X should display a fivefold greater flux than Nafion115.

Using same experimental procedure as the Nafion115 tests, all the experiments for X as well employed 80ml acrylic jars (Beauticom) partially filled with an aqueous solution of PA. As before, the jars were then placed in an inverted configuration in a 400ml beaker filled with 3% saltwater (by weight) such that the membrane stayed submerged in the beaker.

Two kinds of X membranes were tested: X-normal and X-special. Since membrane X is thinner and more fragile than Nafion115, it was decided not to subject it to convective flow and therefore only the beaker test was performed. Tests were conducted at three temperatures: room temperature (22°C), 40°C and 50°C.

#### 3.2 Lists of experiments for membrane X

Preliminary tests were conducted to gain a basic understanding of membrane X-normal as follows:

Table 3.1 Preliminary tests for ‘X’

Temperature (°C)	PA concentration (%)	Saltwater concentration (%)
22	33	3
22	20	3

Next, tests were conducted with both X membranes at the highest PA concentration:

Table 3.2 Comparison tests for two kinds of ‘X’

Temperature	Membrane	PA concentration (%)	Saltwater concentration (%)
22	X- normal	66.7	3
50			
22	X- special		
50			

Next, additional tests were conducted with X-normal to increase the concentration range.

Table 3.3 Concentration gradient tests for X-normal

Temperature (°C)	PA concentration (%)	Saltwater concentration (%)
22	66.7	3
	40	
	20	
40	66.7	
	40	
	20	

Then, tests were conducted to gauge the effect of a temperature gradient across the membrane since it is hypothesized that warm saltwater and cool PA should enhance water flux.

Table 3.4 Temperature gradient tests for X-normal

Temperature of PA solution (°C)	Temperature of saltwater (°C)	PA concentration (%)	Saltwater concentration (%)
22	40	66.7	3
40			

Finally, considering the different physical properties of PA and Ionic Liquid (IL), a similar experiment was performed to assess the behavior of IL.

Table 3.5 Repeated tests of temperature gradient for IL

Temperature of Ionic Liquid (°C)	Temperature of saltwater (°C)	Saltwater concentration (%)
22	22	3
40	40	
22	40	
40	22	

### 3.3 Data and analysis for membrane X

Similar to the Nafion115 tests, the mass of liquid in the jar was recorded as a function of time. Due to the higher water transfer rates with X (about 10 times that of Nafion115), sampling times for X were reduced to 1 hour, and even 20 minutes in some cases.

Here, we plot the mass of liquid inside jar vs. time, concentration vs. time and flux vs. time curves for the four tests listed above. Each test employed membrane samples that were cut from sheets manufactured at different times, and therefore there is some variability in the results that makes the results difficult to compare.

#### 3.3.1 Room temperature test

Figure 3.1 shows the gain in water mass with time for membrane X-normal at room temperature starting with PA concentrations of 33% and 20%.

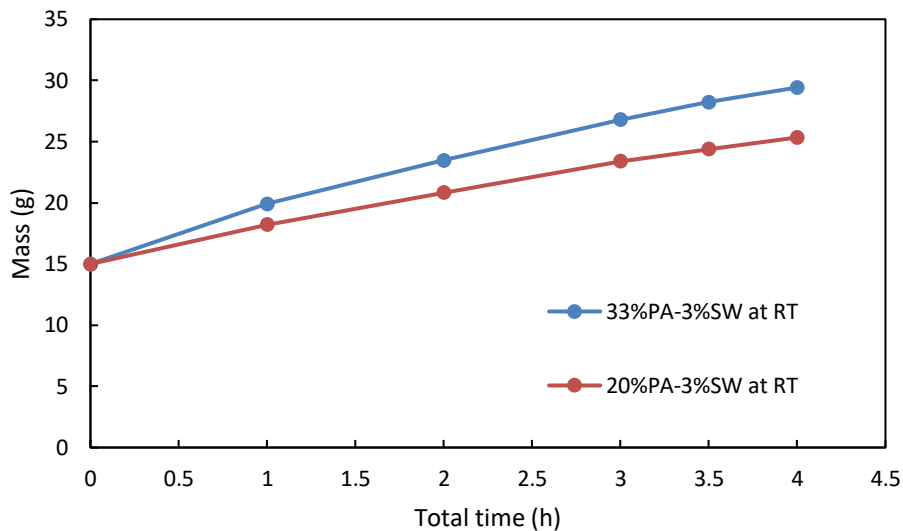


Figure 3.1 Preliminary tests for X-normal at room temperature (22°C)

It is immediately apparent that the water transferability for X-normal is greatly superior to Nafion115. For example, while it took 24 hours for Nafion115 to go from an initial liquid mass of 15g to 22.85g at room temperature, it only took one hour for X-normal to go from 15g to 19.9g at 33% PA. Thus, the time duration for experiments with membrane X can be greatly reduced which speeds up the data collection.

### 3.3.2 Comparison of X-normal with X-special

Figure 3.2 and 3.3 show water absorption with time for X-normal and X-special, respectively. Data was collected with a starting PA concentration of 66.7% for 22°C and 50°C. The initial mass of PA solution was again fixed 15g, and the concentration of PA was fixed at the highest possible concentration (66.7%) to accelerate water mass gain for the different materials.

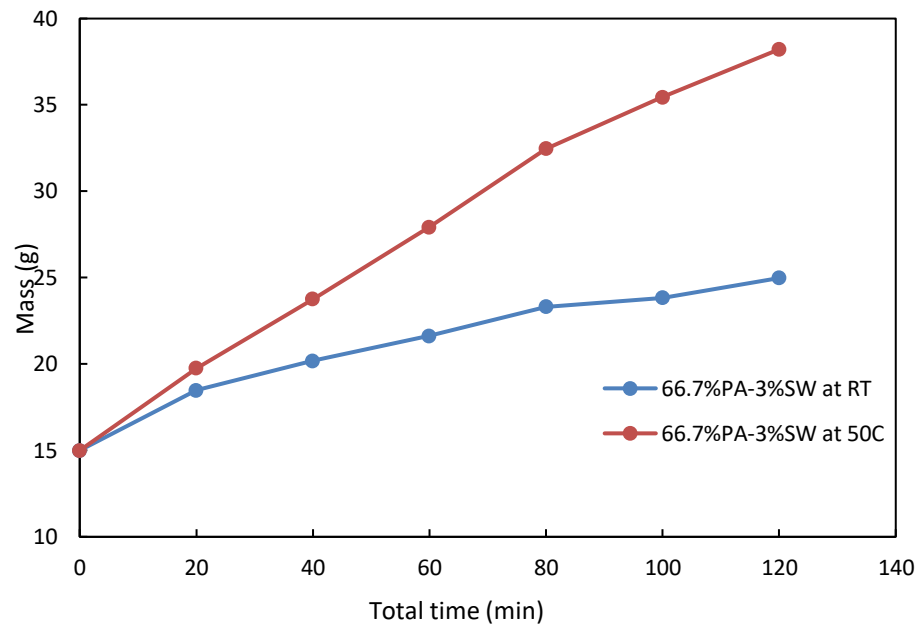


Figure 3.2 Water transferability for X-normal at 22°C and 50°C.

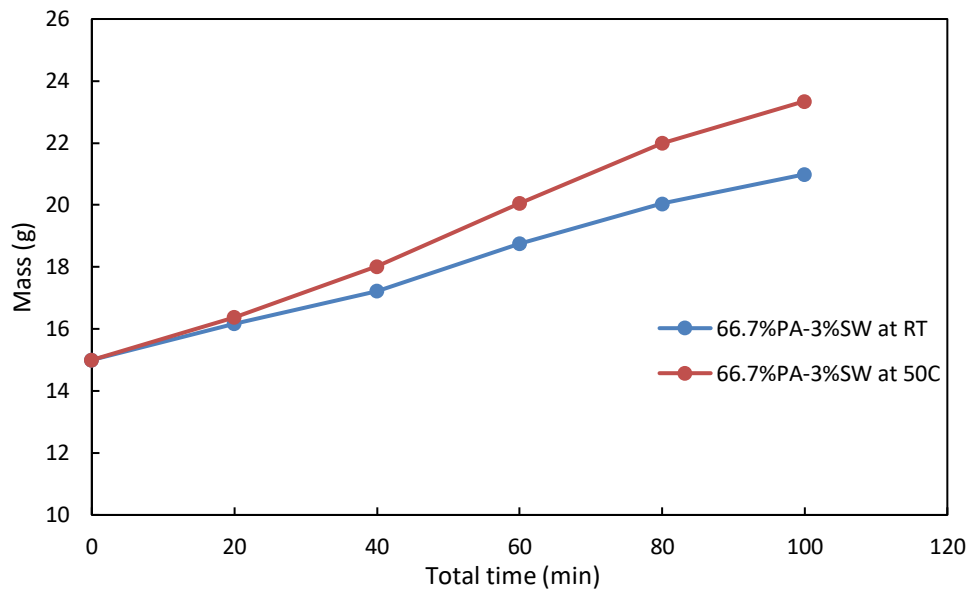


Figure 3.3 Water transferability for X-special at 22°C and 50°C.

The results indicate that X-normal possesses a higher water transferability than X-special. At 50°C, X-normal absorbed 20.45g of water while X-special only absorbed 8.35g of water after 100 min from the saltwater solution. At room temperature, X-normal took up 8.83g of water while X-special took up 5.99g after 100 min. It may be concluded that X-normal has much greater water absorption compared to X-special, and the difference between the two is much higher at 50°C. However, X-special is more stable at higher temperatures which could be useful for future research. Since the design temperature for the current application is 40-60°C (solar heating), X-normal was selected for subsequent experiments.

X-normal possesses a better water transferability than X-special; as shown in Figures 3.5, the average flux for X-normal is around  $1.25 \times 10^{-4} g/cm^2 \cdot s$ , while it is only  $5 \times 10^{-5} g/cm^2 \cdot s$  for X-special. It can be concluded that the water transferability of X-normal is more than twice that of X-special.

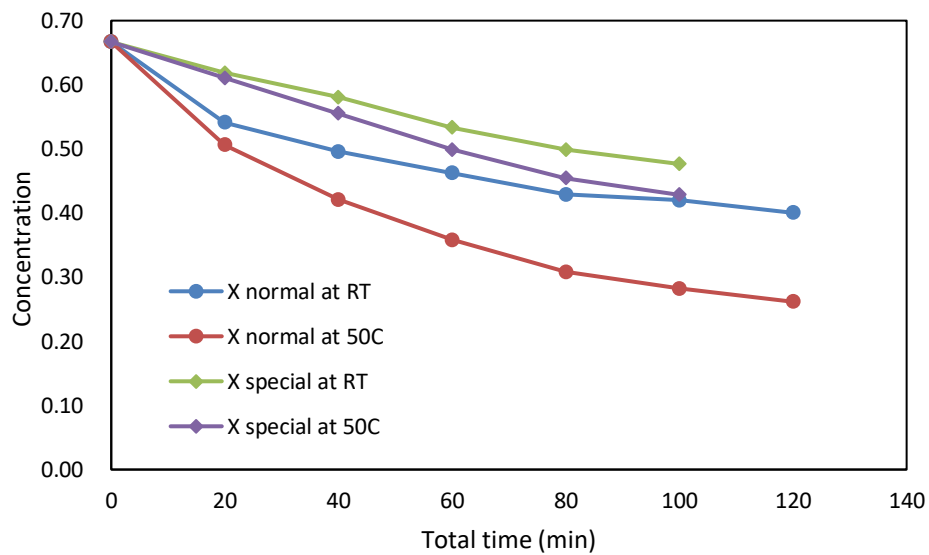


Figure 3.4 Concentration versus time for both X membranes at RT and 50°C; all experiments employed 66.7% PA solution with 3% saltwater.

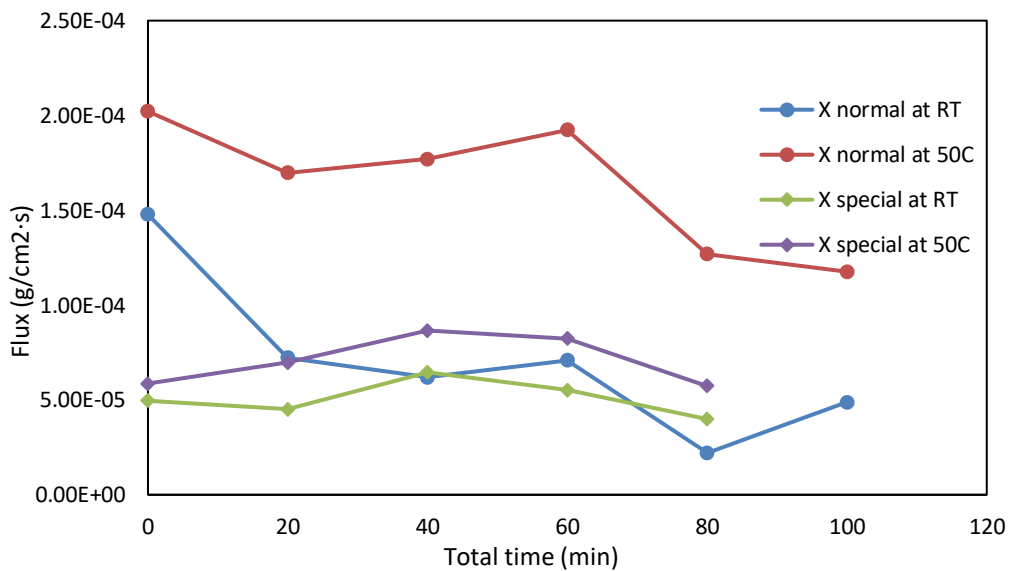


Figure 3.5 Flux versus time for both X membranes at RT and 50°C; all experiments employed 66.7% PA solution with 3% saltwater.

### 3.3.3 Additional tests with X-normal for various PA concentrations

Based on the previous data, it was decided to conduct additional experiments by varying PA concentrations. Figures 3.6 and 3.7 show water gain with time for X-normal at 22 and 40°C, respectively. In each case, three starting PA concentrations were employed: 20%, 40% and 66.7%. Moreover, the initial mass of PA solution was fixed at 40g to improve the resolution of the concentration versus time curves.

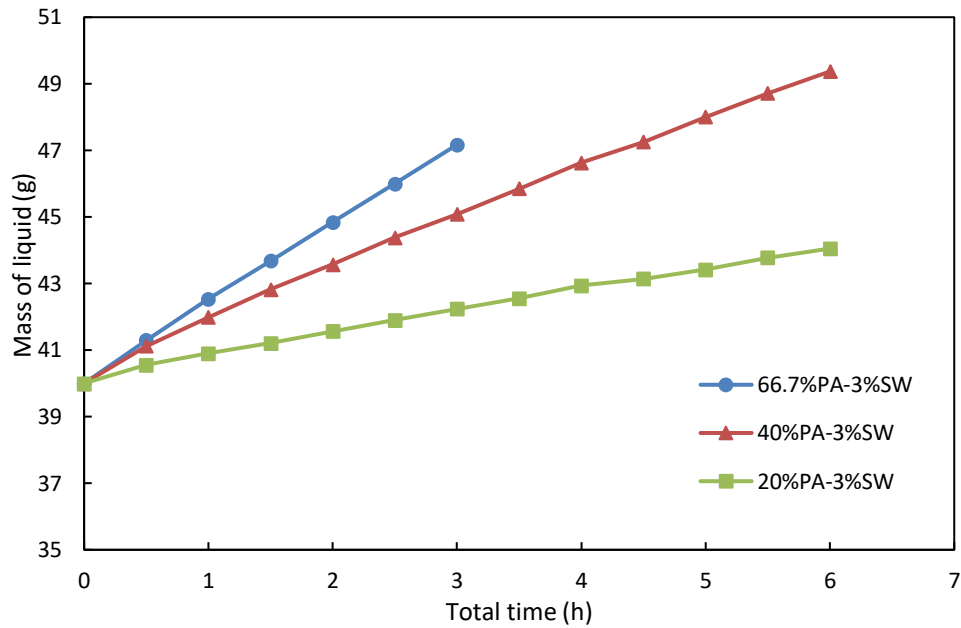


Figure 3.6 Additional tests with X-normal at 22°C, initial weight of liquid was set to 40g.

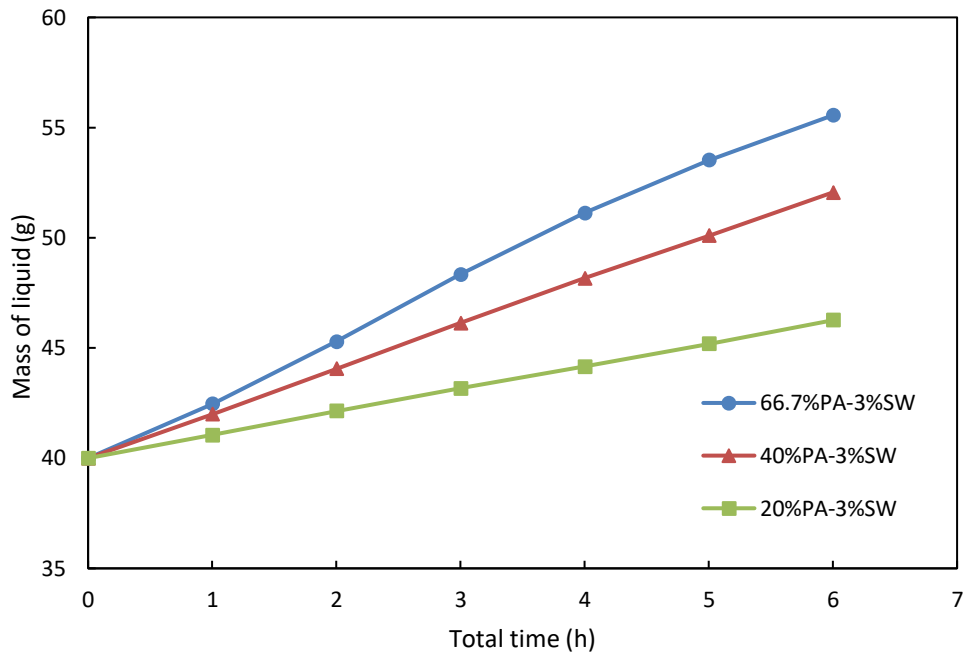


Figure 3.7 Additional tests with X-normal at 40°C, initial weight of liquid controlled at 40g.

The results from these tests are not as promising as the earlier tests. It is seen that with temperature increase from 22°C to 40°C, in 3 hours, the water absorbed by the 66.7% PA concentration only increased from 7.17g to 8.33g. This is significantly smaller than the water uptake shown in Figures 3.2 and 3.3. We attribute the big drop in water uptake to inconsistencies in the manufacture of the membrane.

We plot the PA concentration in tests for X-normal as a function of time at 22 and 40°C in Figure 3.8. The 40% PA concentration curves are offset from the 66.7% curves by about 8 hours, and the 20% PA concentration curves are offset from the 40% curves by about 14 hours. This offset was obtained by just eye-balling the two sets of curves such that they overlaid each other to the best possible extent. We then

plot the water flux vs. time for X-normal at 22 and 40°C in Figure 3.9. The same offsets used in the concentration vs. time curves are employed in the flux versus time curves as well.

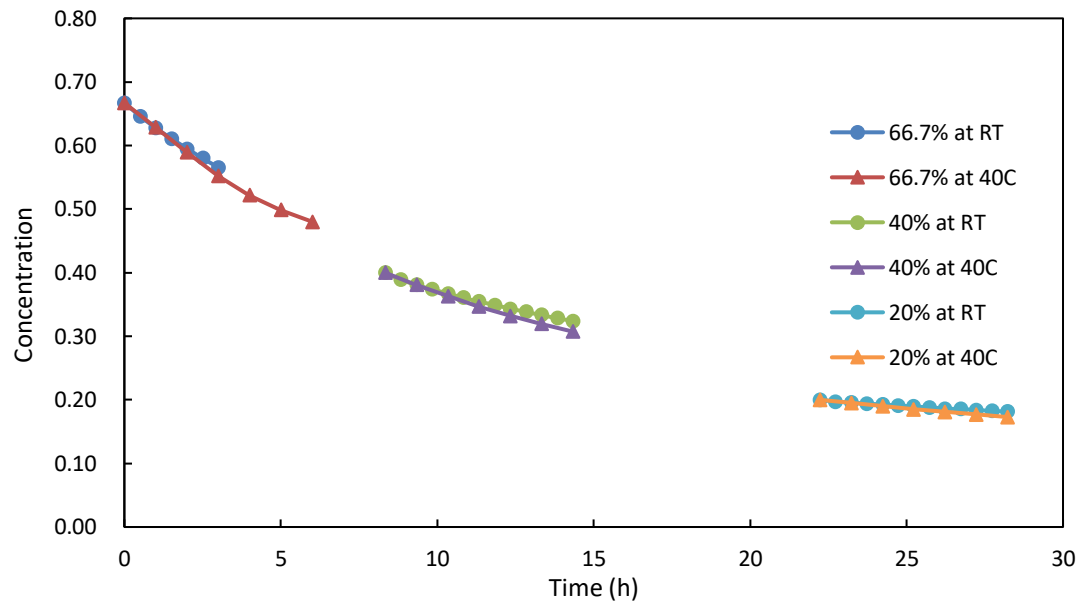


Figure 3.8 Concentration versus time for X-normal at room temperature group and 40°C.

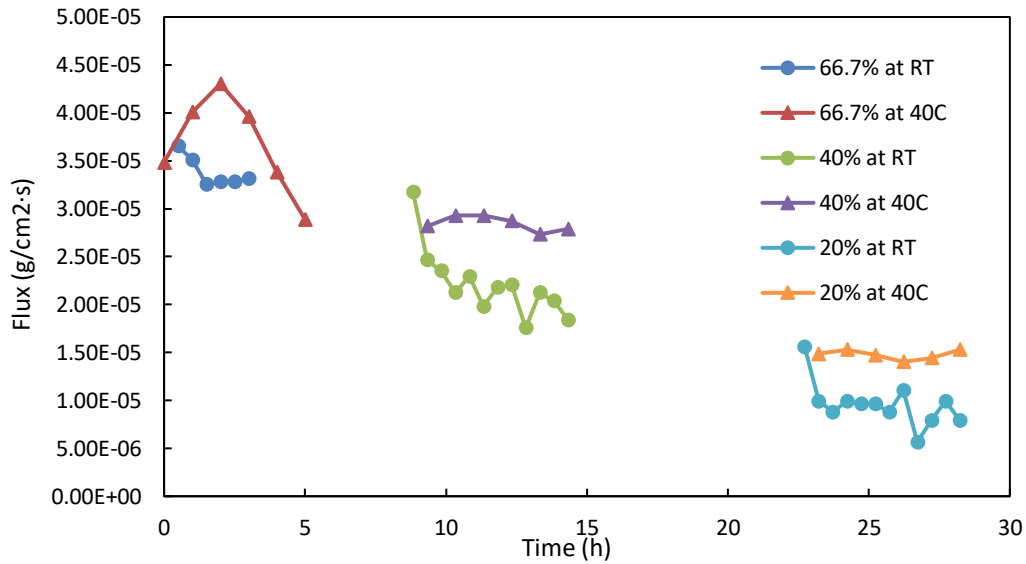


Figure 3.9 Flux versus time for X-normal at room temperature group and 40°C.

Figure 3.8 shows that Group [3] produces cleaner concentration versus time curves. By using proper time offsets, it is possible to make all the curves for different initial PA concentrations merge smoothly.

Figure 3.9 shows that the flux for X-normal and 20%-66.7% PA varies from  $1.0$  to  $4.5 \times 10^{-5} \text{ g/cm}^2 \cdot \text{s}$ , which is much higher than that of Nafion membranes ( $2.56$  to  $3.54 \times 10^{-6} \text{ g/cm}^2 \cdot \text{s}$  at  $20^\circ\text{C}$  for 25%-30% PA with 3% SW). For X normal, increasing the temperature from  $22^\circ\text{C}$  to  $40^\circ\text{C}$  will increase the flux by about  $5 \times 10^{-6} \text{ g/cm}^2 \cdot \text{s}$ , which is not a huge increase.

As shown in Figures 3.8 and 3.9, the measured flux of samples in group [2] and [3] are  $1.75 \times 10^{-4} \text{ g/cm}^2 \cdot \text{s}$  and  $3.75 \times 10^{-5} \text{ g/cm}^2 \cdot \text{s}$ , respectively. Clearly there is a huge gap between the performance of group [2] and [3], which is puzzling.

### 3.3.4 Effect of temperature gradient across the membrane for PA solution

In Figure 3.10, we show results for two experiments: (1) both saltwater and PA solution heated at 40°C, and (2) only saltwater heated at 40°C and PA solution at room temperature. The experiments were performed as follows. For (1) we simply placed the beaker inside the oven at the prescribed temperature. For (2) the temperature conditions were slightly more difficult to maintain because after the cold PA solution is placed inside the warm saltwater beaker, the PA solution warms up within about 20 minutes. Therefore, experiment (2) had to be conducted in an intermittent manner such that after every weight measurement, the PA solution was again cooled back to room temperature by placing it in an ice water bath. We anticipated that the PA solution will accept water less readily when it is heated. To our surprise, experiment (1) showed better water transferability than experiment (2).

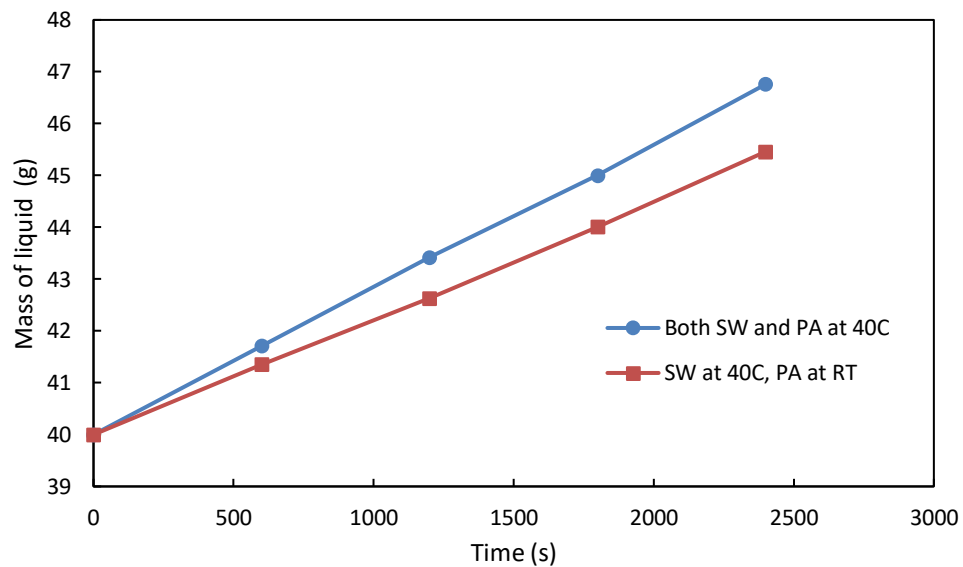


Figure 3.10 Dilution of PA solution versus time for two situations: (1) both saltwater and PA solution heated, and (2) only saltwater heated.

Therefore, our hypothesis that warm saltwater and cool PA would enhance the water flux was not verified. Figure 3.11 shows the variation of concentration versus time for the two experiments. Figure 3.12 shows the average flux for ‘both SW and PA at 40°C’ and ‘SW at 40°C, PA at RT’ groups as  $1.44 \times 10^{-4} g/cm^2 \cdot s$  and  $1.16 \times 10^{-4} g/cm^2 \cdot s$ , respectively, which indicates that the ‘both heated’ case transfers water 20% better than the ‘SW at 40°C, PA at RT’ case.

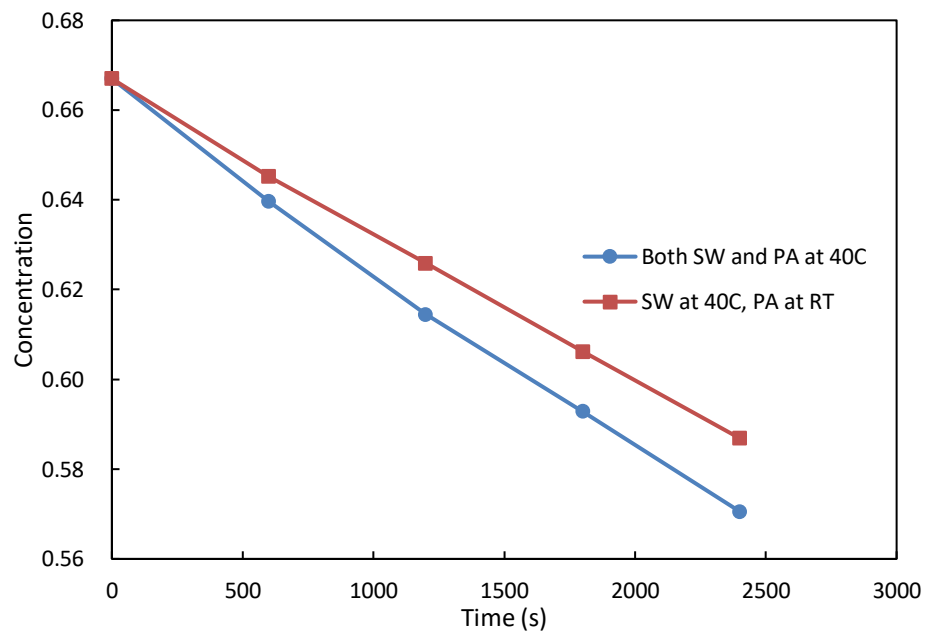


Figure 3.11 Concentration versus time comparing “both SW and PA at 40°C” and “SW at 40°C, PA at RT” cases for X-normal.

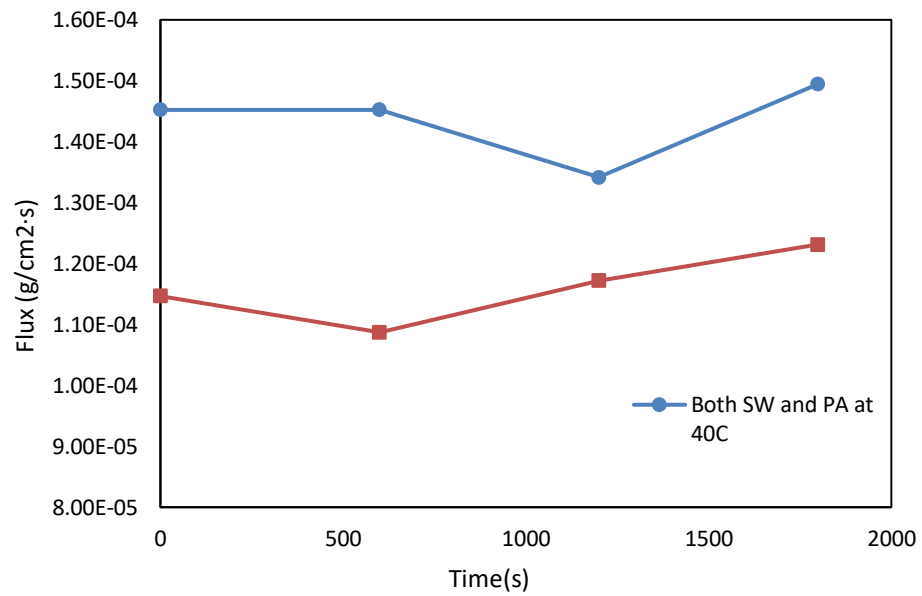


Figure 3.12 Flux versus time comparing “both SW and PA at 40°C” and “SW at 40°C, PA at RT” cases for X-normal.

### 3.3.5 Effect of temperature gradient across the membrane for ionic liquid (1-Ethyl-3-methylimidazolium acetate, CAS:[143314-17-4])

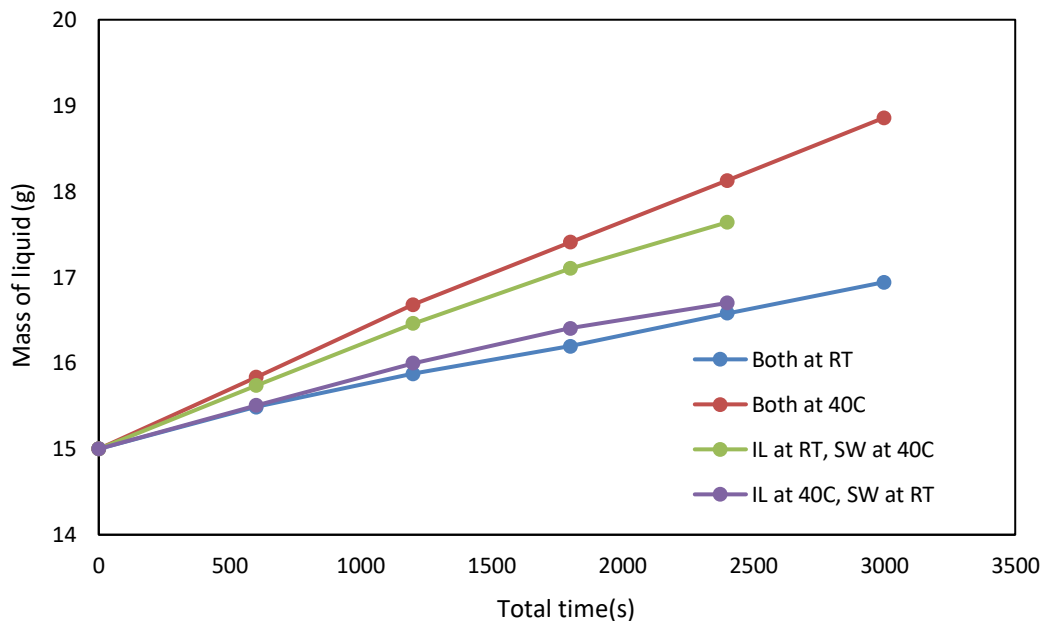


Figure 3.13 Dilution of ionic liquid versus time for four situations: (1) both IL and SW at room temperature; (2) both IL and SW at 40°C; (3) IL at RT, SW at 40°C; and (4) IL at 40°C, SW at 40°C .

The results described in 2.3.4 above for PA were surprising in that the temperature gradient (saltwater heated with PA solution RT) did not lead to a higher water transfer rate. We suspected that PA solution has different properties than the ionic liquid which would actually be used in our desalination system. Therefore, we repeated the experiments in 2.3.4 with ionic liquid. Since evaporation increases with temperature for ionic liquid, we expected water transferability into the ionic liquid to increase for the forward osmosis case where the ionic liquid is at room temperature with saltwater heated. Figure 3.13 shows that the “Both at RT” case exhibited the

lowest water transferability which is expected. However, the “Both at 40°C” group still performs the best which is consistent with the PA results in Figure 3.10. For the other two groups, “IL at RT-SW at 40°C” performs better than “IL at 40°C-SW at RT” which matches our expectation.

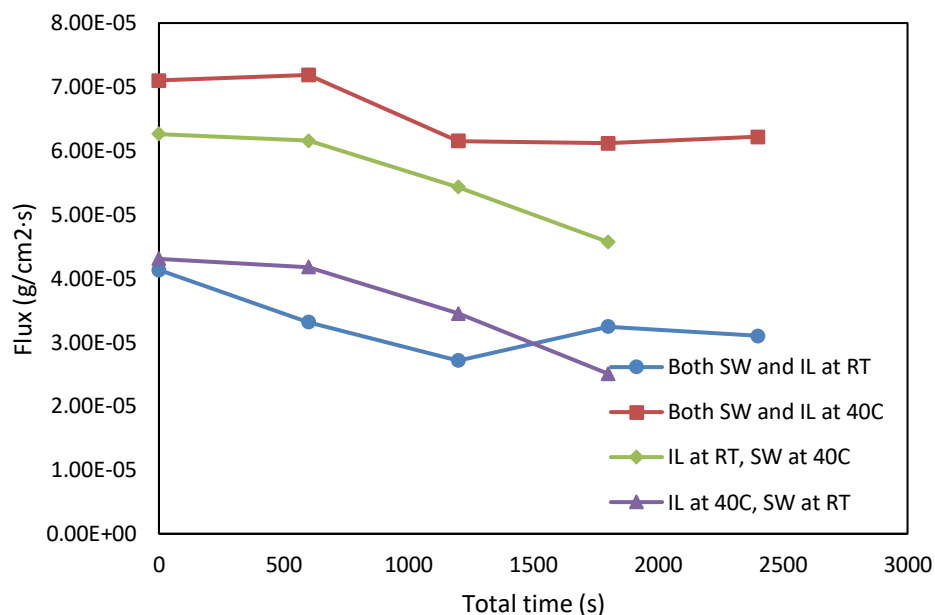


Figure 3.14 Flux versus time for four cases with X-normal and ionic liquid.

The flux-time curves in Figure 3.14 confirm that the “Both heated” group possesses the highest water transferability, and “Both at RT” group shows the lowest water transferability. Comparing the flux-time curve with result of PA in Figure 3.12, the average computed flux for IL varied from  $3.30\sim 6.55 \times 10^{-5} g/cm^2 \cdot s$ , whereas the flux for PA varied from  $1.16\sim 1.44 \times 10^{-4} g/cm^2 \cdot s$ . Thus it can be concluded that the water transferability for IL is lower than that for 66.7% PA solution.

These results require careful explanation. There are two effects that are prevalent in this experiment. First, it is well known that the water diffusivity of PFSA membranes improves with temperature. Therefore, it stands to reason that the best performer is when both liquids (and therefore the membrane as well) are heated to 40°C. Second, our belief is that heated ionic liquid is less accepting of water than room temperature ionic liquid. Therefore, a temperature gradient where ionic liquid is at room temperature with saltwater heated should promote water migration. However, it is not clear if the temperature gradient is really playing a significant role. Although the “IL at RT-SW at 40°C” performs better than “IL at 40°C-SW at RT”, we need to realize that the mass of the SW is much greater than the mass of the ionic liquid. Hence, in both these cases, the membrane temperature is influenced more by the SW temperature rather than the IL temperature. Therefore, although heating the IL apparently slows water migration, since the SW mass is much greater than the IL mass, we can infer that the membrane temperature in the “IL at 40°C-SW at RT” drops more quickly and so the lower water transferability observed could be due to the effect of temperature on the PFSA membrane’s water diffusivity.

Interestingly, Figure 3.14 shows that there are some similarities between the shapes of the “both at RT” and “both at 40°C” curves; likewise, the curves for “IL at RT, SW at 40°C” and “IL at 40°C, SW at 40°C” are also relatively similar. For ‘Both at 40°C’ and ‘Both RT’, it maybe concluded that the higher water transfer ability of the system come with higher temperature and evaporation of water inside heated IL balanced each other after second data point, the flux curve might keep the shape until the balance is broken. For ‘IL at 40°C, SW at 40°C’ and ‘IL at RT, SW at 40°C’, it was supposed that the experiment has not arrived the equilibrium point between

temperature and evaporation effect, and evaporation dominate the experiment in current stage. Obviously, a complete curve including more data point is necessary to study the effect of temperature gradient and evaporation in the future.

## Chapter 4

### MODELLING OF FORWARD OSMOSIS

In this chapter we apply modelling to analyze the water flux across membranes under various conditions. The goal of this chapter is to build a model of forward osmosis across membranes to predict water flux and compare with experimental data in future work. We will begin by modelling of the experiments in Section 3.1 for membrane 'X'.

#### 4.1 Basic modelling for experiments in 3.1

In the experiments in Section 3.1, the liquid made contact with the membrane as shown in Figure 4.1. The water flux is driven by the difference of osmotic pressure in saltwater (SW) and the potassium acetate solution (PA).

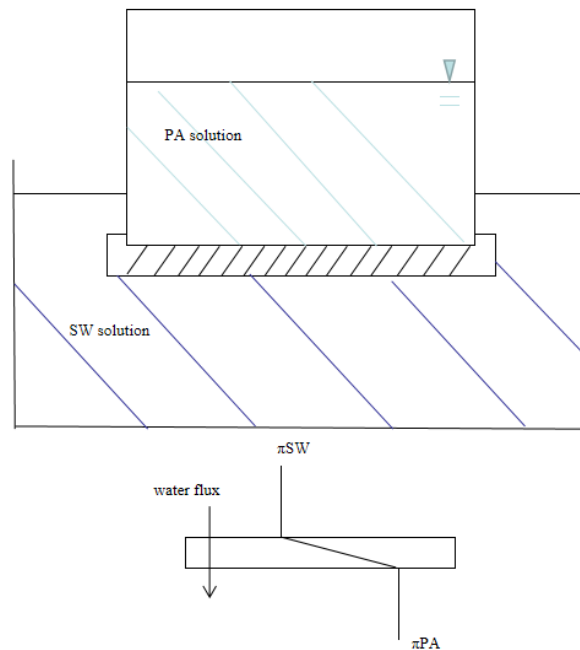


Figure 4.1 Experimental setup in 3.1 (top); and water flux across the membrane driven by pressure difference (bottom),  $\pi_{PA}$  and  $\pi_{SW}$  represent the osmotic pressures in PA and SW solutions, respectively.

Here we consider an ideal condition: no concentration polarization and no solute (potassium acetate and salt) flux; thus, the only flux that needs to be considered here is the water flux from SW to PA across the membrane.

$$J_v = A(\sigma\Delta\pi - \Delta P) \quad (4.1)$$

where  $A$  is membrane water permeability coefficient ( $\text{m}^3/(\text{m}^2 \text{ s Pa})$ ),  $\sigma$  is the reflection coefficient, which is usually assumed to be unity, and  $\Delta P$  is applied hydraulic pressure, which is equal to 0 in our forward osmosis setup. Hence:

$$J_v = A(\pi_{draw} - \pi_{feed}) \quad (4.2)$$

From van't Hoff theory<sup>[13]</sup>,

$$\pi = cRT \quad (4.3)$$

where  $c$  is the molar concentration of solute,  $R$  is the ideal gas constant, and  $T$  is the temperature in K. Substituting Equation 4.3 in 4.2, we obtain:

$$J_v = ART(c_{draw} - c_{feed}) \quad (4.4)$$

$J_v$  is calculated in Chapters 1 and 2, and  $C_{draw}$ ,  $C_{feed}$ , and  $T$  are set parameters.

Hence, we can solve for  $A$ .

Thus, we obtain a basic model for ideal forward osmosis.

## 4.2 Modelling of forward osmosis in a tube flow

A typical forward osmosis system would consist of a shell-and-tube mass transfer apparatus, where the ionic liquid (or PA solution) would flow through the tube extracting water from the surrounding seawater in the shell. In order to model this system, let us consider the tube flow shown in Figure 4.2.

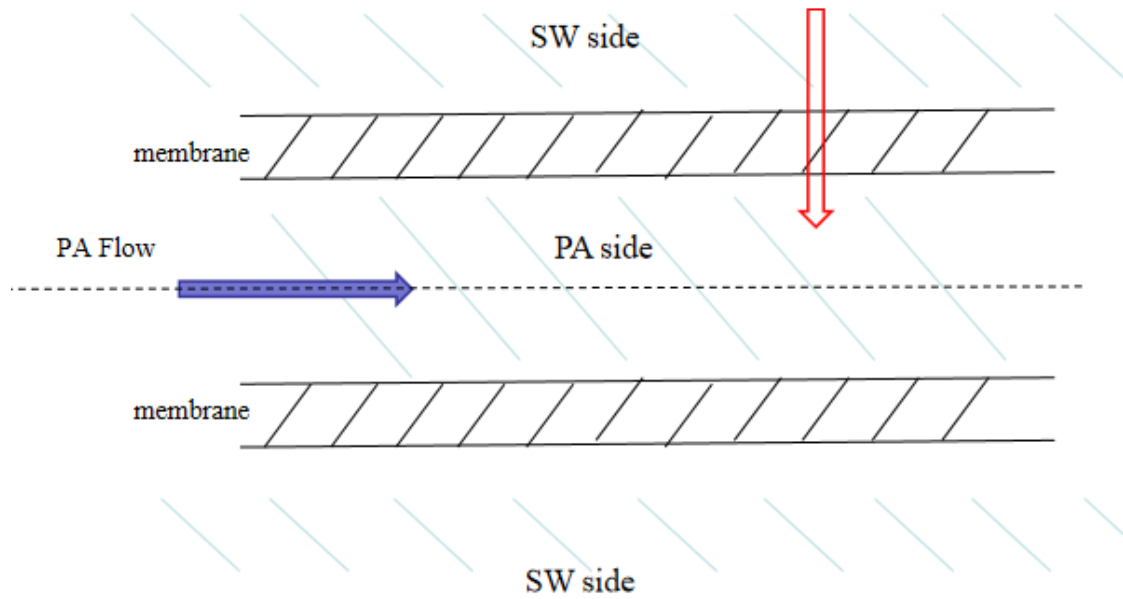


Figure 4.2 Schematic of tube flow for modeling purposes

For the tube flow, there is no water accumulation in the membrane wall, therefore the water flow into the membrane from the SW side is balanced by the water flow out of the membrane on the PA side. Figure 4.3 shows the details.

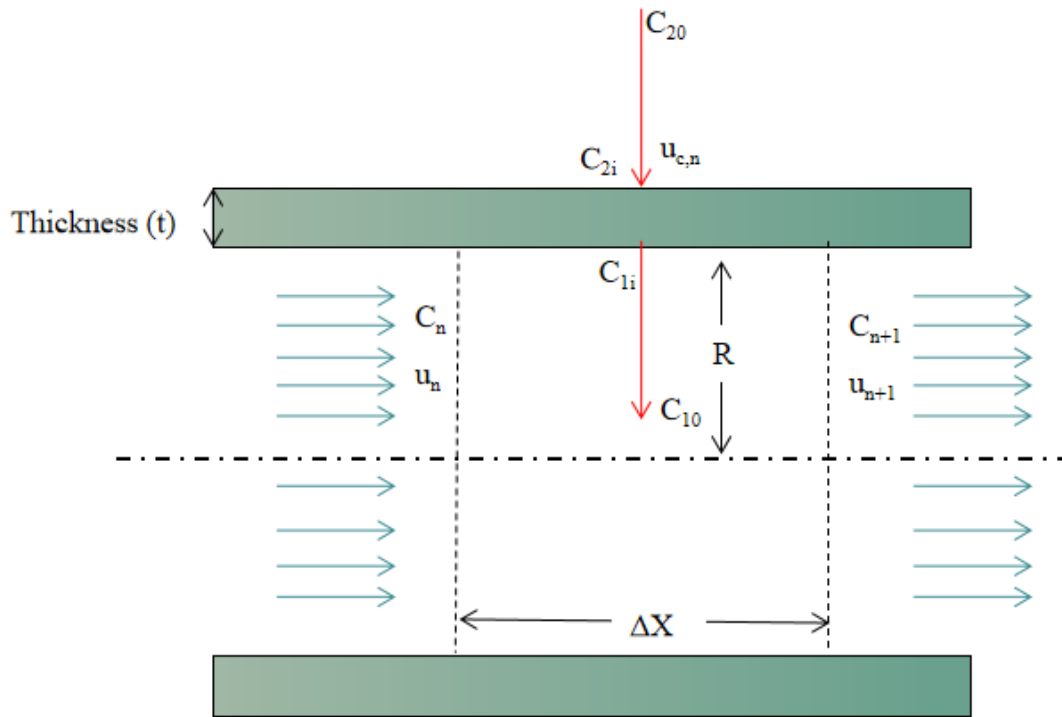


Figure 4.3 Analysis of forward osmosis in a tube flow.  $C_{20}$  and  $C_{2i}$  represent the bulk and interfacial water concentration on the SW side, respectively.  $C_{10}$  and  $C_{1i}$  represent the bulk and interfacial water concentration on the PA side.  $R$  is the tube radius.  $C_n$  and  $C_{n+1}$  represent the concentration of PA ( $\text{g/cm}^3$ ) at the entry and exit of the control volume, respectively.  $u_{c,n}$  represents the velocity of water entering the control volume across the tube wall.  $u_n$  and  $u_{n+1}$  represent the velocity of PA solution flow at the entry and exit of the control volume, respectively.

Our experiments have confirmed that the volume of PA solution is given by:

$$Vol = \frac{m_{PA} + m_w}{\rho_w}$$

Thus, the concentration of PA can be written as:

$$C_n = \frac{m_{PA}}{Vol} = \frac{m_{PA}}{\frac{m_{PA} + m_w}{\rho_w}}$$

The mass concentration of water in PA solution, which is a function of  $x$ , can be written as:

$$C_m = \frac{m_w}{m_{PA} + m_w} = 1 - \frac{C_n}{\rho_w} \quad (4.5)$$

Let us consider the water flux across the membrane from the SW to the PA solution.

Water flux at the SW side:

$$u_{c,n} = K_{sw}(C_{20} - C_{2i,n}) \quad (4.6)$$

Water flux across the membrane:

$$u_{c,n} = \frac{D}{t}(C_{2i,n} - C_{1i,n}) \quad (4.7)$$

Water flux at the PA side:

$$u_{c,n} = K_{PA}(C_{1i,n} - C_{10,n}) \quad (4.8)$$

In Equations 4.6-4.8,  $u_{c,n}$  is the water flux (cm/s) which is a function of  $x$ ,  $K_{sw}$  and  $K_{PA}$  are the mass transfer coefficients (cm/s),  $D$  is the diffusion coefficient (cm<sup>2</sup>/s) of water in the membrane obtained from experiments in Chapter 3, and  $t$  is the thickness of the membrane (cm).

Combining Equations 4.5-4.7, we obtain:

$$C_{20} - C_{10,n} = u_{c,n} \left( \frac{1}{K_{sw}} + \frac{t}{D} + \frac{1}{K_{PA}} \right) \quad (4.9)$$

To simplify, we rewrite the total mass transfer resistance  $\left( \frac{1}{K_{sw}} + \frac{t}{D} + \frac{1}{K_{PA}} \right)$  as  $\alpha$ :

$$C_{20} - C_{10,n} = u_{c,n}\alpha \quad (4.10)$$

Using Equation 4.5, this can be rewritten as:

$$C_{20} - \left(1 - \frac{c_n}{\rho_w}\right) = u_{c,n}\alpha$$

Therefore,

$$u_{c,n} = \frac{c_{20} - \left(1 - \frac{c_n}{\rho_w}\right)}{\alpha} \quad (4.11)$$

Applying mass conservation of water to the control volume in Figure 4.3, we obtain:

$$(u_{n+1} - u_n)\pi R^2 = 2\pi R\Delta x u_{c,n}$$

Therefore:

$$u_{n+1} = u_n + u_{c,n} \frac{2\Delta x}{R} \quad (4.12)$$

Applying mass conservation of PA to the control volume in Figure 4.3, we obtain:

$$u_n C_n = u_{n+1} C_{n+1}$$

Therefore:

$$C_{n+1} = \frac{u_n C_n}{u_{n+1}} \quad (4.13)$$

Substituting Equations 4.11 and 4.12 into 4.13, we obtain:

$$C_{n+1} = \frac{u_n C_n}{u_n + \left(c_{20} - \left(1 - \frac{c_n}{\rho_w}\right)\right) \frac{2\Delta x}{R\alpha}} \quad (4.14)$$

In Equation 4.14,  $C_{20}$ , the initial values of  $C_n$  and  $u_n$ , and  $\Delta x$  are input values, and  $\alpha$  can be determined using values for  $K_{SW}$  and  $K_{PA}$  obtained from the literature or from the experiments in Chapter 3.  $\rho_w = 1.0 \text{ g/cm}^3$  and  $R = 0.5 \text{ cm}$ . Thus, we can solve numerically for the bulk water mass concentration on the PA side,  $C_m(x)$ .

### 4.3 Effect of parameter variation on simulation results

Here, we will employ Equation 4.14 to solve for  $C_n$  using Matlab. In Equation 4.14,  $C_{20}$  is the bulk concentration of water on the SW side, which is fixed as 0.97, an average value for seawater. The initial value of  $C_n$  is known as the initial bulk concentration of PA on the PA side at the beginning of test in Figure 4.2. Assuming 66.7 wt.% for PA (the saturation concentration of PA in water at room temperature) in Figure 4.2, the initial value of  $C_n = 0.667$ .

Next, we determine the value of  $K_{SW}$  and  $K_{PA}$  as follows:

$$K = \frac{D}{l} \tag{4.15}$$

where  $D$  is the diffusivity of a solute in water and  $l$  is the mass transfer boundary layer thickness. In Equation 4.15,  $D_{SW}$  and  $D_{PA}$  are assumed to be around  $1\text{E-}5 \text{ cm}^2/\text{s}$ <sup>[12]</sup>.  $l$  is assumed as 0.01cm. Therefore, the baseline value of  $K_{SW}$  and  $K_{PA}$  is  $1\text{E-}3 \text{ cm/s}$ . However, to study its effect on mass transport, we will use three different values of  $K_{SW}$  and  $K_{PA}$  as  $1\text{E-}2$ ,  $1\text{E-}3$ , and  $1\text{E-}4 \text{ cm/s}$ . The mass transfer resistance of the membrane wall is  $t/D$ , where  $t$  is the known thickness of the Xergy membrane (0.0025 cm), and  $D$  is diffusion coefficient of water in the membrane, which is estimated from the experimental results in Chapter 3 as  $4\text{E-}6 \text{ cm}^2/\text{s}$ .  $\Delta x$  was selected by performing grid convergence studies.

We will now introduce the Reynolds number to represent the initial PA flow velocity:

$$Re = \frac{uD}{\nu} \quad (4.16)$$

In Equation 4.16,  $\nu$  is the kinematic viscosity of PA solution at 20°C, which is 0.1 cm<sup>2</sup>/s<sup>[14]</sup>.  $D$  is the diameter of the tube, given as 1 cm. We will let  $Re$  take on the values of 1, 10, and 100 giving  $u_n = 0.1, 1, \text{ and } 10$  cm/s, respectively.

Profiles of  $C_m(x)$  for varying  $K_{SW}$  and  $K_{PA}$  for  $Re = 10$  are shown in Figure 4.4, and profiles of  $C_m(x)$  for varying  $Re$  for  $K_{SW} = K_{PA} = 10^{-3}$  cm/s are shown in Figure 4.5.

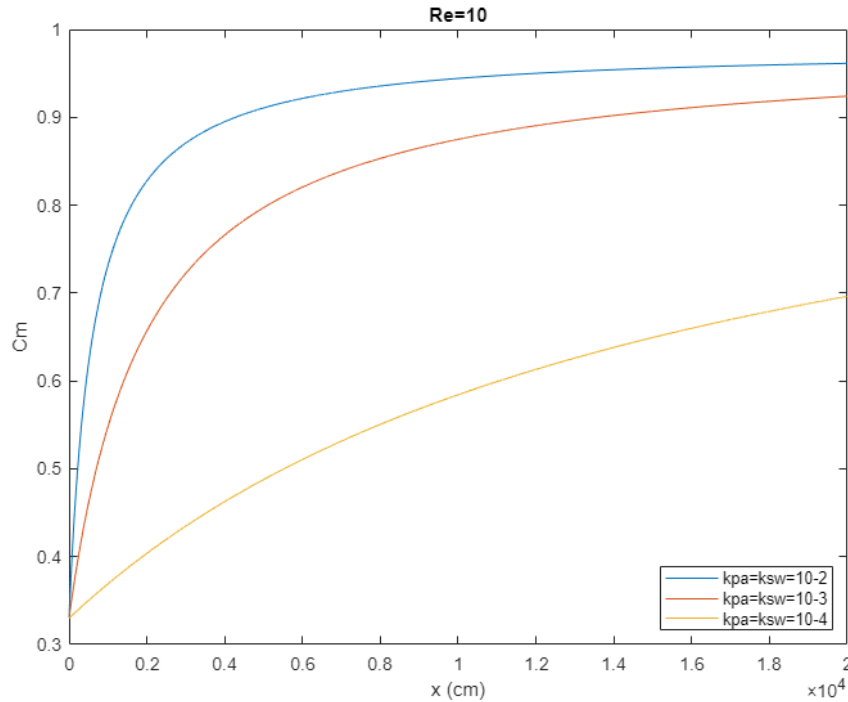


Figure 4.4 Profiles of  $C_m(x)$  for varying  $K_{SW}$  and  $K_{PA}$  for  $Re = 10$ .

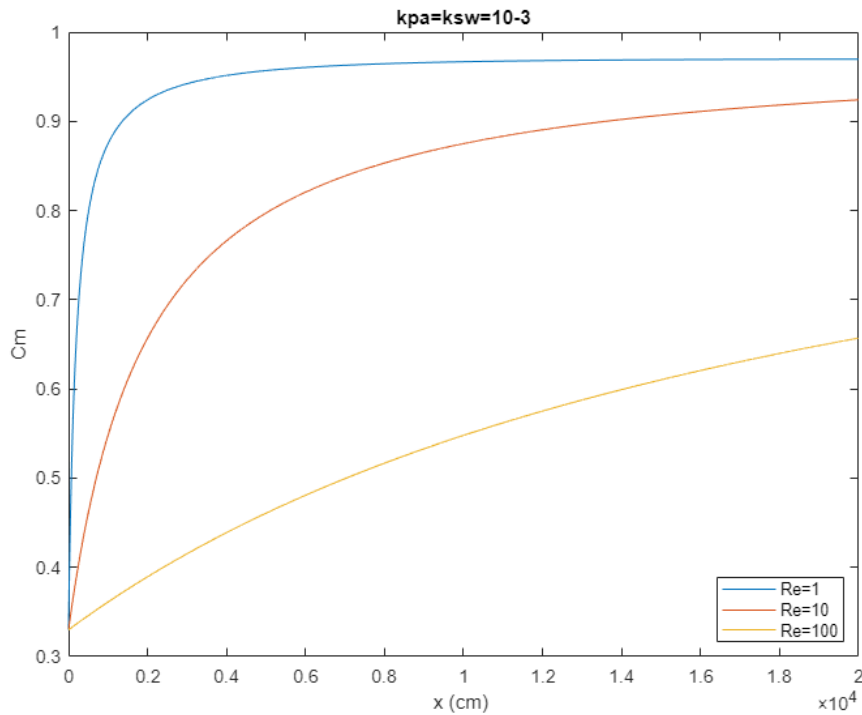


Figure 4.5 Profiles of  $C_m(x)$  for varying  $Re$  for  $K_{SW} = K_{PA} = 10^{-3}$  cm/s.

The modelling results in Figures 4.4 and 4.5 show that the bulk water concentration with the tube on the PA side is highly sensitive to both the mass transfer coefficients and  $Re$ . A small  $Re$  and a large mass transfer coefficient cause the PA solution to dilute faster and reach its equilibrium value of 0.97 more rapidly. This result can be explained quite easily. A smaller  $Re$  implies that the residence time of the fluid within the same length of tube is higher allowing the dilution as a function of  $x$  to increase. Likewise, a higher mass transfer coefficient also accelerates dilution. These results can provide valuable guidelines for the design of the mass transfer apparatus.

## Chapter 5

### CONCLUSIONS AND FUTURE WORK

#### 5.1 Conclusions

In this thesis, the effect of both temperature and PA concentration on water transport by forward osmosis across Nafion115 and proprietary membranes from Xergy was studied. Results in Chapters 2 and 3 consistently show that the forward osmosis efficiency increases with both temperature and PA concentration. Comparing results of the beaker test and tank test in Chapter 2, it is apparent that disrupting boundary layer on the SW side of the membrane has a very small effect on the rate of water transport. From this we may conclude that most of the resistance to water transport comes from the membrane itself. Comparing water flux data for all the three membranes tested (Nafion115, X-normal, X-special), X-normal provides the highest water flux. Although it was hypothesized that a temperature gradient across the membrane with hotter SW and cooler PA/ionic liquid would improve transport, on the contrary, results showed that a higher overall temperature produced the greatest water transport. This is attributed to the increase in water diffusivity through the membrane at higher temperature.

Modelling of the mass transfer based on Fick's Law and mass conservation confirmed that dilution of the flow in the tube increases when the Reynolds number is reduced and when the mass transfer coefficient is increased.

#### 5.2 Future work

All the experiments conducted in this thesis pertained to water transport measurements across planar films under static conditions. However, any practical application would employ a shell-and-tube type mass transfer apparatus. The modeling

in Chapter 4 represents the first step in constructing some design guidelines for future experiments. Such experiments would need to be performed to validate the model. Additional tasks for the future would include membrane durability studies, as well as energy optimization for the overall desalination process depicted in Figure 1.6.

## REFERENCES

1. Worldwide wildlife-water scarcity. [Online], available at: (<https://www.worldwildlife.org/threats/water-scarcity>).
2. Ghaffour, Noreddine; Missimer, Thomas M.; Amy, Gary L. (January 2013). "Technical review and evaluation of the economics of water desalination: Current and future challenges for better water supply sustainability". *Desalination*. 309: 197–207. doi:10.1016/j.desal.2012.10.015
3. Schematic of MSF. [Online], available at : ([https://en.wikipedia.org/wiki/Multi-stage\\_flash\\_distillation](https://en.wikipedia.org/wiki/Multi-stage_flash_distillation))
4. Saadat, A H M & Islam, Md Saiful & Fahmida, Parvin & Sultana, Ayesha. (2018). Desalination Technologies for Developing Countries: A Review. *Journal of Scientific Research*. 10. 77-97.
5. Smith, Maurice (October 2008), "Watershed moment: SAGD operators embrace new water treatment options", *Air Water Land*, retrieved 11 December 2014.
6. Warsinger, David & Mistry, Karan & Nayar, Kishor & Chung, Hyung Won & V, John. (2015). Entropy Generation of Desalination Powered by Variable Temperature Waste Heat. *Entropy*. 17. 7530-7566. 10.3390/e17117530.
7. Davis, T.A., "Electrodialysis", in *Handbook of Industrial Membrane Technology*, M.C. Porter, ed., Noyes Publications, New Jersey (1990).
8. Electrodialysis. [Online], available at: ([https://en.wikipedia.org/wiki/Electrodialysis#cite\\_note-Davis-1](https://en.wikipedia.org/wiki/Electrodialysis#cite_note-Davis-1))
9. WHAT IS REVERSE OSMOSIS AND HOW DOES IT WORK? [Online], available at: (<https://www.evoqua.com/en/brands/IPS/Pages/what-is-reverse-osmosis.aspx>)
10. T.V. Nguyen and R.E. White, *J. Electrochem. Soc.* 140, (1993) 2178.
11. Q. Duan, H. Wang, J. Benziger, Transport of liquid water through Nafion membranes, *J. Membr. Sci.* 392–393 (2012) 88-94.
12. Cussler, Edward Lansing, and Edward Lansing Cussler. *Diffusion: mass transfer in fluid systems*. Cambridge university press, 2009.
13. Wikipedia. [online], available at : ([https://en.wikipedia.org/wiki/Van\\_%27t\\_Hoff\\_equation](https://en.wikipedia.org/wiki/Van_%27t_Hoff_equation))

14. Potassium Acetate Fact Sheet by CRYOTECH.

## **Appendix A**

### **MATLAB FUNCTION OF MODELLING USED IN 4.3**

## A.1 Function for varying $K_{SW}$ and $K_{PA}$ .

```
1 -   clc;
2 -   clear all;
3 -   close all;
4 -   num = 20000;
5 -   output_1 = zeros(num,4);
6 -   output_2 = zeros(num,4);
7 -   output_3 = zeros(num,4);
8
9   %%%%%%%%%%%%%%%%%%%%%%%%%%%%%%%%%%%%%%%%%%%%%%%%%%%%%%%%%%%%%%%%%%%%%%%%%
10 -  x = 0;
11 -  pw = 1;
12 -  t = 25e-4;
13 -  D = 4e-6;
14 -  c20 = 0.97;
15 -  delta_x = 1;
16 -  cn = 0.67;
17 -  R = 0.5;
18 -  un = 1;
19 -  cm = 1-cn;
20
21 -  kpa = 1e-2;|
22 -  ksw = kpa;
23 -  alpha = 1/ksw + t/D + 1/kpa;
24   %%%%%%%%%%%%%%%%%%%%%%%%%%%%%%%%%%%%%%%%%%%%%%%%%%%%%%%%%%%%%%%%%%%%%%%%% loop %%%%%%%%%%%%%%%%%%%%%%%%%%%%%%%%%%%%%%%%%%%%%%%%%%%%%%%%%%%%%%%%%%%%%%%%%
25
26 -  for i = 1:num
27 -      output_1(i,1) = cn;
28 -      output_1(i,2) = x;
29 -      output_1(i,3) = log10(x);
30 -      output_1(i,4) = cm;
31 -      x = x + delta_x;
32 -      cn = un*cn/(un+(c20-(1-cn/pw))*2*delta_x/alpha);
33 -      cm = 1-cn;
34 -  end
```

```

35
36 %%%%%%%%%%%%%%%%%%%%%%%%%%%%%%%%%%%%%%%%%%%%%%%%%%%%%%%%%%%%%%%%%%%%%%%%%
37 - x = 0;
38 - pw = 1;
39 - t = 25e-4;
40 - D = 4e-6;
41 - c20 = 0.97;
42 - delta_x = 1;
43 - cn = 0.67;
44 - R = 0.5;
45 - un = 1;
46 - cm = 1-cn;
47
48 - kpa = 1e-3;
49 - ksw = kpa;
50 - alpha = 1/ksw + t/D + 1/kpa;
51 %%%%%%%%%%%%%%%%%%%%%%%%%%%%%%%%%%%%%%%%%%%%%%%%%%%%%%%%%%%%%%%%%%%%%%%%% loop %%%%%%%%%%%%%%%%%%%%%%%%%%%%%%%%%%%%%%%%%%%%%%%%%%%%%%%%%%%%%%%%%%%%%%%%%
52 - for i = 1:num
53 -     output_2(i,1) = cn;
54 -     output_2(i,2) = x;
55 -     output_2(i,3) = log10(x);
56 -     output_2(i,4) = cm;
57 -     x = x + delta_x;
58 -     cn = un*cn/(un+(c20-(1-cn/pw))*2*delta_x/alpha);
59 -     cm = 1-cn;
60 - end
61
62 %%%%%%%%%%%%%%%%%%%%%%%%%%%%%%%%%%%%%%%%%%%%%%%%%%%%%%%%%%%%%%%%%%%%%%%%%
63 - x = 0;
64 - pw = 1;
65 - t = 25e-4;
66 - D = 4e-6;
67 - c20 = 0.97;
68 - delta_x = 1;
69 - cn = 0.67;

```

```

70 - R = 0.5;
71 - un = 1;
72 - cm = 1-cn;
73
74 - kpa = 1e-4;
75 - ksw = kpa;
76 - alpha = 1/ksw + t/D + 1/kpa;
77 - Re = 100;
78 - %%%%%%%%%%%%%%% loop %%%%%%%%%%%%%%%
79 - ksw = kpa;
80 - for i = 1:num
81 -     output_3(i,1) = cn;
82 -     output_3(i,2) = x;
83 -     output_3(i,3) = log10(x);
84 -     output_3(i,4) = cm;
85 -     x = x + delta_x;
86 -     cn = un*cn/(un+(c20-(1-cn/pw))*2*delta_x/alpha);
87 -     cm = 1-cn;
88 - end
89
90 - figure;
91 - plot(output_2(:,2),output_1(:,4),...
92 -     output_2(:,2),output_2(:,4),...
93 -     output_2(:,2),output_3(:,4));
94 - % xlabel('$\log_{10}x$ (cm)');
95 - xlabel('x (cm)');
96 - ylabel('Cm');
97 - legend('kpa=ksw=10-4','kpa=ksw=10-5','kpa=ksw=10-6','location','southeast');
98 - title('Re=10');
99

```

## A.2 Function for varying $Re$

```
1 - |clc;
2 -   clear;
3 -   close all;
4 -   num = 20000;
5 -   output_1 = zeros(num,4);
6 -   output_2 = zeros(num,4);
7 -   output_3 = zeros(num,4);
8
9   %%%%%%%%%%%%%%%%%%%%%%%%%%%%%%%%%%%%%%%%%%%%%%%%%%%%%%%%%%%%%%%%%%%%%%%%%
10 -  x = 0;
11 -  pw = 1;
12 -  t = 25e-4;
13 -  D = 4e-6;
14 -  c20 = 0.97;
15 -  delta_x = 1;
16 -  cn = 0.67;
17 -  R = 0.5;
18
19 -  un = 0.1;
20
21 -  cm = 1-cn;
22 -  kpa = 1e-3;
23 -  ksw = kpa;
24 -  alpha = 1/ksw + t/D + 1/kpa;
25   %%%%%%%%%%%%%%%%%%%%%%%%%%%%%%%%%%%%%%%%%%%%%%%%%%%%%%%%%%%%%%%%%%%%%%%%% loop %%%%%%%%%%%%%%%%%%%%%%%%%%%%%%%%%%%%%%%%%%%%%%%%%%%%%%%%%%%%%%%%%%%%%%%%%
26
27 -  for i = 1:num
28 -     output_1(i,1) = cn;
29 -     output_1(i,2) = x;
30 -     output_1(i,3) = log10(x);
31 -     output_1(i,4) = cm;
32 -     x = x + delta_x;
33 -     cn = un*cn/(un+(c20-(1-cn/pw))*2*delta_x/alpha);
34 -     cm = 1-cn;
```

```

35 - end
36 - %%%%%%%%%%%%%%%%%%%%%%%%%%%%%%%%%%%%%%%%%%%%%%%%%%%%%%%%%%%%%%%%%%%%%%%%%
37 -
38 - x = 0;
39 - pw = 1;
40 - t = 25e-4;
41 - D = 4e-6;
42 - c20 = 0.97;
43 - delta_x = 1;
44 - cn = 0.67;
45 - R = 0.5;
46 -
47 - un = 1;
48 -
49 - cm = 1-cn;
50 - kpa = 1e-3;
51 - ksw = kpa;
52 - alpha = 1/ksw + t/D + 1/kpa;
53 -
54 - %%%%%%%%%%%%%%%%%%%%%%%%%%%%%%%%%%%%%%%%%%%%%%%%%%%%%%%%%%%%%%%%%%%%%%%%% loop %%%%%%%%%%%%%%%%%%%%%%%%%%%%%%%%%%%%%%%%%%%%%%%%%%%%%%%%%%%%%%%%%%%%%%%%%
55 - for i = 1:num
56 -     output_2(i,1) = cn;
57 -     output_2(i,2) = x;
58 -     output_2(i,3) = log10(x);
59 -     output_2(i,4) = cm;
60 -     x = x + delta_x;
61 -     cn = un*cn/(un+(c20-(1-cn/pw))*2*delta_x/alpha);
62 -     cm = 1-cn;
63 - end
64 - %%%%%%%%%%%%%%%%%%%%%%%%%%%%%%%%%%%%%%%%%%%%%%%%%%%%%%%%%%%%%%%%%%%%%%%%%
65 - x = 0;
66 - pw = 1;
67 - t = 25e-4;
68 - D = 4e-6;

```

```

69 - c20 = 0.97;
70 - delta_x = 1;
71 - cn = 0.67;
72 - R = 0.5;
73
74 - un = 10;
75
76 - cm = 1-cn;
77 - kpa = 1e-3;
78 - ksw = kpa;
79 - alpha = 1/ksw + t/D + 1/kpa;
80 %%%%%%%%%%%%%%% loop %%%%%%%%%%%%%%%
81 - ksw = kpa;
82 - for i = 1:num
83 -     output_3(i,1) = cn;
84 -     output_3(i,2) = x;
85 -     output_3(i,3) = log10(x);
86 -     output_3(i,4) = cm;
87 -     x = x + delta_x;
88 -     cn = un*cn/(un+(c20-(1-cn/pw))*2*delta_x/alpha);
89 -     cm = 1-cn;
90 - end
91 %%%%%%%%%%%%%%%
92
93 - figure;
94 - plot(output_1(:,2),output_1(:,4),...
95 -     output_2(:,2),output_2(:,4),...
96 -     output_3(:,2),output_3(:,4));
97 - xlabel('x (cm) ');
98 - % xlabel('$x$ (cm)');
99 - ylabel('Cm');
100 - legend('Re=1', 'Re=10', 'Re=100', 'location', 'southeast');
101 - title('kpa=ksw=10-3');

```

## Appendix B

### COPYRIGHT PERMISSION OF FIGURES

<b>Description</b>	Schematic of a multistage evaporator A - Steam in, B - Seawater in, C - Potable water out, D - Waste out, E - Steam out, F - Heat exchange, G - Condensation collection, H - Brine heater
<b>Date</b>	29 January 2010, 17:30 (UTC)
<b>Source</b>	<ul style="list-style-type: none"><li>Multiflash.png</li></ul>
<b>Author</b>	<ul style="list-style-type: none"><li>Multiflash.png: Ruben Castelnuovo (myself)</li><li>derivative work: NJR_ZA (talk)</li></ul>

I, the copyright holder of this work, hereby publish it under the following licenses:

This file is licensed under the [Creative Commons Attribution-Share Alike 2.5 Generic](#), [2.0 Generic](#) and [1.0 Generic](#) license.

You are free:



- **to share** – to copy, distribute and transmit the work
- **to remix** – to adapt the work



Under the following conditions:

- **attribution** – You must give appropriate credit, provide a link to the license, and indicate if changes were made. You may do so in any reasonable manner, but not in any way that suggests the licensor endorses you or your use.
- **share alike** – If you remix, transform, or build upon the material, you must distribute your contributions under the same or compatible license as the original.

This file is licensed under the [Creative Commons Attribution-Share Alike 3.0 Unported](#) license.

You are free:



- **to share** – to copy, distribute and transmit the work
- **to remix** – to adapt the work



Under the following conditions:

- **attribution** – You must give appropriate credit, provide a link to the license, and indicate if changes were made. You may do so in any reasonable manner, but not in any way that suggests the licensor endorses you or your use.
- **share alike** – If you remix, transform, or build upon the material, you must distribute your contributions under the same or compatible license as the original.

This licensing tag was added to this file as part of the GFDL licensing update.



Permission is granted to copy, distribute and/or modify this document under the terms of the [GNU Free Documentation License](#), Version 1.2 or any later version published by the Free Software Foundation; with no Invariant Sections, no Front-Cover Texts, and no Back-Cover Texts. A copy of the license is included in the section entitled [GNU Free Documentation License](#).



I, the creator of this work, hereby grant the permission to copy, distribute and/or modify this document under the terms of the [GNU Free Documentation License](#), Version 1.2 or any later version published by the Free Software Foundation; with no Invariant Sections, no Front-Cover Texts, and no Back-Cover Texts. Subject to disclaimers.



This work is licensed under the [Creative Commons Attribution-Share Alike 3.0 License](#).



This licensing tag was added to this file as part of the GFDL licensing update.